QATAR UNIVERSITY

COLLEGE OF ARTS AND SCIENCES

MOLECULAR LEVEL UNDERSTANDING OF NANOCLAY DISPERSION IN POLYSULFONE, POLYIMIDE, AND THEIR BLEND COMPOSITES

BY

NOUR MUNEER BADER

A THESIS SUBMITTED TO THE FACULTY OF

COLLEGE OF ARTS AND SCIENCES

IN PARTIAL FULFILLMENT

OF THE REQUIREMENTS

FOR THE DEGREE OF

MASTER OF SCIENCE

MATERIAL SCIENCE AND TECHNOLOGY

JUNE 2016

COMMITTEE PAGE

The members of the Committee approve the project of Nour Muneer Bader defended on 26 of May, 2016.

_____

Ahmed Elzatahry

Thesis Supervisor

_____

Mariam A. Al-Maadeed

Committee Member

_____

Adriaan Luyt

Committee Member

_____

Mohammad K. Hassan

Committee Member

_____

Karim Alamgir

Committee Member

Approved:

Eiman Mustafawi, Dean, College of Arts and Sciences

ABSTRACT

Polymer composites based on polysulfone (PSF) and polyimide (PI) are used as membranes for gas separation and water purification applications. However, structure composition related issues limit the performance of the used films in those applications. Consequently, the use of nanoclays as reinforcing agents in polymer films can be essential for the membrane's optimal performance. In this work, we will study the effect of a nanoclay, Cloisite 30B, on the dynamics of chain motions of the PSF and PI polymers. Characterization of the PI/PSF/Clay composites will be carried out using the broadband dielectric spectroscopy, SEM, gas separation analysis, and dynamic mechanical analyzer techniques.

The main goal behind this study will be understanding chain relaxation behavior in the glass transition (Tg) and the sub-Tg regions. The impact of the clay on the gas barrier and gas separation properties will also be investigated. Dielectric spectroscopy is a powerful tool to characterize the composites for the following reasons: (1) Polymer chain dynamics related to glass transitions and secondary motions can be studied. For example, two glass transition temperatures would reflect a 2-phase system and this information is related to phase separated morphology results. (2) Distributions of relaxation times can be used to study microstructural heterogeneity within the blend.

Insertion of clay is expected to alter the dynamics of the glass transition temperature and secondary relaxations of polysulfone and polyimide composites. Therefore, clay would alter free volume within the composites and affect the physical aging phenomena in membranes, and thus, their performance in gas separation applications.

TABLE OF CONTENTS

LIST OF FIGURES

LIST OF TABLES

ACKNOWLEDGEMENTS

I am grateful to many people whom, without their support or cooperation, this work would have never been accomplished in its final form.

First and foremost I would like to express my heartfelt gratitude towards my supervisor Dr. Ahmed Elzatahry for granting me the chance to work under his supervision and also for his academic guidance, support, and encouragement during my research work. He gave me his precious time and advice whenever I needed it.

Furthermore, I would like to thank the rest of my thesis committee, Prof. Adriaan Stephanus Luyt, and his research assistant (Ms. Sumaia Algasmi), and Prof. Alamgir Karim for their insightful comments and encouragement, and also for the hard question which incented me to widen my research from various perspectives. I would like to thank Prof. Karim also for his supervision and access to the laboratories and research facilities during training period at Akron University, United States.

I would like to thank Mr. Ali Ammar from the University of Akron for his unlimited help and for all of the useful information and techniques he taught me.

My sincere thanks also goes to Dr. Mohamed Hassan, who guided me through dielectric measurements. Without his precious support it would not be possible to complete this research successfully.

I am also grateful to Prof. Mariam Al-Maadeed, who provided me an opportunity to join the Materials Science and Technology program team as graduate assistant, and gave me access to the laboratory and research facilities at Center of Advanced Materials (CAM).

I would like to thank Materials Science and Technology program for giving me the opportunity to visit the University of Akron, Unites States, as an exchange student and train there. And for the opportunity to participate in a conference in Dubai.

Finally, I would like to express my deepest gratitude to my friends especially Alaa Hassiba for her encouragement and support throughout my thesis.

Last, but by no means least, I thank God.

DEDICATION

I dedicate this thesis to my first teachers in my life, the ones who taught me the first lessons and kept giving me with unconditional love, to my mom and dad.

To my beloved husband, whom without his support, patience, and most of all, love, the completion of this work would have never been possible.

To my lovely mother in law, who keeps supporting me with all the help I need and prayers.

To my greatest gift from God, my kids.

CHAPTER 1

1. INTRODUCTION

Recently, reports have shown that Qatar is considered as one of the largest exporters of liquefied natural gas in the world [1]. According to the *Oil & Gas Journal*, "in 2015, Qatar had the third-largest proved reserves of natural gas in the world at 872 trillion cubic feet (Tcf). Most of Qatar's reserves are in the country's North Field, which is part of the world's largest natural gas deposit" [2].

Given this fact, purification of impurities from natural gas, especially carbon dioxide, is essential as it increases the quality of the natural gas and decreases the corrosion of transportation pipelines [3].

Gas separation is a significant process used by industrial gas suppliers, petroleum processes, chemical industries and refiners [4]. Gas separation plays a very important role in several industrial applications such as natural gas sweetening, H_2 removal from hydrocarbon gases, and O_2/N_2 separation [5]. In addition, food, beverage, cosmetics, electronics and pharmaceutical industries utilize thin polymer membranes for packaging applications that have a controlled gas barrier to protect the products from gases and moisture [6].

Polymer clay nanocomposites (PCN) have shown optimistic results in gas barrier and gas separation properties [7–13]. In addition, industry has shown great potential for

use of polymer clay nanocomposites materials due to clay's enhancement of polymer mechanical and thermal properties [14–16].

Polyimide (PI) composites in general are one of the most commonly used polymer membrane materials and its gas barrier properties have been widely studied for gas separation and packaging applications [17–21]. Prior research studied microporous materials such as zeolite and carbon molecular sieves as a filler for polyimide[22–24]. Layered silicate material has also attracted researchers to use it as filler because of its clear exfoliation effect on the morphology of polymers in general [25–28]. Other studies showed that the addition of low loadings of silicate sheets of montmorillonite had an obvious result in lowering the gas permeation properties of PI membrane [29, 30].

Another polymer that has attracted interest is polysulfone (PSF), which has been used as a barrier for gas separation. PSF is a glassy polymer that is commonly used due to its gas transport properties. These properties have been further improved by loading the polymer with porous inorganic fillers [31]. In 2002, Wang et al. [32] developed a polymer-zeolite system with enhanced interfacial compatibly and relatively few imperfections by using zeolite porous nanocrystals. The system saw an increase in the oxygen permeability of 0.5 barrer and an increase in the selectively of O_2/N_2 of 1.8. In 2007, another study was conducted featuring PSF by Kim et al. [33] where the membranes were loaded with adjusted 10Å porous nanotubes of carbon. In this case, the oxygen permeability and O_2/N_2 selectivity increased by 0.39and 0.28 barrer, respectively. The CO_2 permeability increased by 1.3 barrer while selectively of CO_2/CH_4 decreased by 6.

In this work, polyimide/Cloisite 30B and polysulfone/Cloisite 30B have been fabricated via a doctor blade casting technique. Both composites were investigated by dielectric spectroscopy to study the effect of clay on the molecular mobility of polymer. The gas separation of both polymers was investigated to calculate the oxygen permeability of the membrane.

Chapter 1 includes the introduction and literature review of gas separation membranes, different gas theory, types of membrane separation, and the role of clay in enhancing barrier properties. Chapter 2 includes materials and experimental techniques used in this work. Chapter 3 presents the results and discussion.

This thesis includes 166 references, 6 tables, and 32 figures.

CHAPTER 2

2. LITRETURE REVIEW

Introduction to literature review

The fundamentals of gas separation were set forth by T. Graham, who completed the first gas separation experiment in a polymeric membrane in 1829 [34]. The first H_2 recovery system using gas separation membrane was established in 1977 by a company called Monsanto/Perma [35]. Various milestones in industrial applications of gas separation membranes have since been achieved. Original membranes were cellulose-based which lead to plasticization in tough flue gas, making cellulose ill-suited for industry [36]. That, however, pushed scientists to investigate new membranes with better permeability, selectivity, and mechanical and thermal durability properties. Several polymeric membranes have resulted with reasonable gas separation performances, such as polyamides, polycarbonate, polysulfones, and polyimides [37, 38].

Polymer membranes are used to filter one or more gases from a feed mixture. The two important properties that affect the performance of the membrane are permeability and selectivity. Both are considered as specific properties for a certain material used to fabricate the membrane. In addition, both have a clear impact on the productivity and the purity efficiency of the membrane.

Permeability is a parameter that describes the flux of gas in the region it occupies, while selectivity is the ability of the membrane to allow the transfusion of one gas while blocking another, as shown in Figure 1.

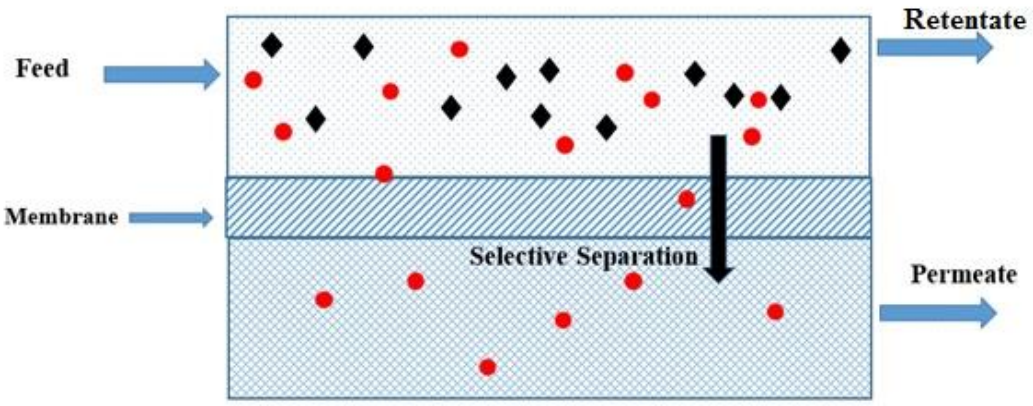

Figure 1 : Principle of gas permeation and separation

Objectives

Developing highly efficient membranes for gas separation has attracted the interest of many scientists both in academia and industry and many studies have been devoted to improve such membranes. Accordingly, the main objectives of this thesis are:

1- Preparare and characterize pulysulfone/clay nanocomposite membranes.

2- Prepare and characterize polyimide/ clay nanocomposites membranes.

3- Use dielectric spectroscopy to study the effect of clay on the sub-T_g and T_g-related relaxation.

4- Evaluate the prepared membranes as oxygen gas barriers.

In this work, two types of nanocomposites (polysulfone/clay and polyimide/clay) are studied with a focus on investigating the application of gas separation technique,

especially as it applies to oxygen permeability. This can be achieved by increasing the distance of the diffusion path, thereby reducing the quantity of oxygen molecules that would permeate through the membrane in a given time. The aim of this thesis is to prove the ability of improving gas barrier based on nanocomposites membranes.

Theory of gas permeation

The permeation of gas through membranes occurs as a result of a pressure gradient. Because the morphology of the membrane restricts the translation of the gas through the membrane, different morphologies have different transport mechanisms [39].

Moreover, varying pore sizes of membranes result in five possible mechanisms for membrane separation [40]: surface diffusion, molecular diffusion (or molecular sieving), capillary condensation, Knudsen diffusion and solution-diffusion separation.

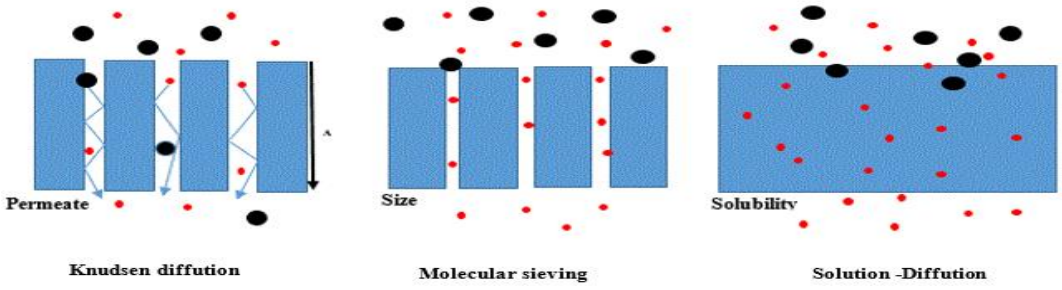

Figure 2: Schematic representation of three of the different possible mechanisms for membrane gas separation, Knudsen diffusion, molecular.

Since polymers have packed chains they are considered to be dense packaging materials that allow for very few permeable corridors for molecules [41]. Molecules need to be dissolved into the polymer matrix and then diffused through it in order to permeate. This solution-diffusion permeation process is defined as:

$$P = D \times S \qquad \text{Equation [1]}$$

where P is the permeability ($cm^3 \cdot cm/ (cm^2 \cdot s \cdot Pa)$), D is diffusivity ($cm^2/s$) and S is the solubility (cm^3 (273.15K; 1.013 × 105 Pa)/$cm^3 \cdot$ Pa) of the polymer. Diffusivity is a kinetic parameter defined as the ability of molecules to pass through a polymer membrane. Solubility is a thermodynamic parameter related to penetrant-polymer interactions. Gas transport is affected by the morphology of the polymer. Diffusion through polymers can exist in two states: they rubbery (below T_g) and glassy state (above T_g).

Polysulfone and Matrimid© polyimide are examples of glassy polymers. The major free volume within the glassy polymeric membranes is due to the presence of micro voids. Membranes comprised of glassy polymers are generally diffusivity and selectivity controlled [42].

1.1.1 Knudsen Diffusion

Knudsen diffusion typically takes place in macroporous and mesoporous membranes. In this mechanism, the pore size of the membrane is smaller than the free path of the gas molecules. In this case, collisions between the molecules and the pore barrier are more frequent than collisions between the molecules themselves. The selectivity is proportional to the inverse square root of the molecular weights [43].

1.1.2 Surface Diffusion

In surface diffusion, gas species are typically adsorbed at the pore barrier. The degree of interaction between the adsorbed gas and pore surface determines the rate of surface diffusion. As a result, separation occurs due to the difference in gas-membrane interactions for various gas. Surface diffusion generally occurs in combination with other transport mechanisms such as Knudsen diffusion [44].

1.1.3 Molecular Diffusion

Molecular diffusion, or molecular sieving, differs from Knudesen diffusion as it occurs when the pore size is larger than the mean free path of the gas species. Here the diffusions happens mainly through collisions between the molecules themselves. The direction of the separation is dictated by the composition gradient. It is referred to as molecular sieving because it works as a sieve for the gas mixture and it depends on size exclusion. In addition, membrane's pore sizes are specified depending on the diameter of the gas molecules. This makes a difference in the rate of diffusion for small molecules as compared to larger ones. For example, the CO_2 /N_2, unity is smaller than the selectivity, as N_2 has a larger kinetic diameter than CO_2 [45].

1.1.4 Capillary Condensation

Capillary condensation is usually detected in mesoporous membranes. It is a type of surface flow that occurs when there is a condensable gas in the mixture and it fills the pore. After that a meniscus is formed at the ends of the pore, it facilitates the transport of

gas through hydrodynamic flow that is caused by a capillary pressure difference between the ends. Regarding the process of adsorption, as pressure is increased, the ultimate limits can be obtained through capillary condensation. Theoretically, this mechanism can achieve very high selectivity, which is due to the liquid layers of condensed gas that this layer will block, inhibiting the flow of non-condensable gases [46].

1.1.5 Solution-diffusion separation

Solution-diffusion separation, also referred to as configurational or microspore diffusion, occurs when the pore size of the membrane is close in size to the molecular gas diameter. In this mechanism, diffusion is known as an “activated” process and separation occurs when there are strong interactions between the pore wall and the gas molecules. Solution-diffusion separation is common in zeolite membranes and carbon molecular sieves as both are micro porous membranes [47].

Moreover, this type of separation can be considered as the main mechanism for separation through dense polymeric membranes [47–50]. The mechanism can be summarized by three steps:

1- Adsorption: where the gas molecules adsorb on the surface of the membrane.

2- Diffusion: where the gas molecules diffuse through the polymer matrix.

3- Evaporation: where the gas molecules evaporate to the exterior.

Based on the previous explanation of gas permeation theory, we can understand the mechanism that polymers follow. Polymers are generally dense packaging materials with

well packed chains that show very limited pathways for molecular diffusion [41]. In glassy polymers, adsorption of gas is a complicated step defined by the combination of Henry's Law and Langmuir's expressions. Accordingly, it is called "dual mode sorption theory". On the other hand, Arrhenius relations are used to define the solubility and diffusivity coefficients [51].

The effect of chemical structure on membrane permeability

Kim et al. [52] reported synthesis of a series of different structures of aromatic polyimides and tested their permeability and selectivity for different pairs of gases (He/CH_4, CO_2/CH_4, N_2/CH_4, and O_2/N_2). Results showed that the chemical structure has an important impact on the permeability and selectivity by the alteration of diffusivity factors. The same group also suggested that despite the increase in permeability being linked with a decrease in selectivity, there are still other options to have other polymers with high permeability and high selectivity. This can be done by designing the intra segmental mobility and intersegmental packing of membranes [52].

Further studies [53], included a series of fluorinated and non-fluorinated polyimides, examined the effect of chemical structure on permeability and selectivity. The study showed interesting results and concluded that the chain packing density has a direct effect on the permeability. Here they found lower packing densities were associated with higher permeabilities [53].

Similarly, different studies related to the use of various polymers have been collected in order to study the relationship between the permeability and separation factor [54]. The study reported that the capability of the polymer to separate the gas is mainly controlled by the diffusion coefficient. When the molecular spacing in the polymer becomes narrower, the permeability decreases as a result of the decreased diffusion coefficient [54].

For glassy polymers, packing density and mobility of polymer chains control the diffusion coefficient and diffusive selectivity. Increasing packing density will decrease the diffusivity selectivity, which depends on the size gradient.

1.1.6 Fractional free volume

Over the past years, scientists have tried to theoretically understand the permeability of polymers. Several important trials have been done to attempt to increase the intrinsic permeability of the polymer by studying the monomer, rigidity, functional groups and chain structure [55].

Permachor is a method developed by Morris [56] that aims to predict the oxygen permeability in a polymeric membrane by calculating the empirical factor for each chemical group, which directly affects the total permeability.

In another study, Bicerano [57] predicted the permeability using two significant parameters; the rotational freedom and the packing density of the polymer. However, Lee [58] developed an equation that correlates the gas permeability with free volume. He

defined the fractional free volume as (V-V◦)/V, where V and V◦ represent the specific volume (reciprocal of the density) and the volume occupied by the polymer molecule, respectively. More experiments proposed that the effects of the polymer structure on permeability is more about the result of varieties in the diffusion coefficient (D) rather than solubility coefficient (S) [59].

Free volume plays a critical role in the diffusion coefficient, more so than any other parameter. Because of this, a relationship between permeability coefficient and free volume has been determined through experiments [60] as follows:

$$P = A \exp(-B/FFV) \qquad \text{Equation [2]}$$

where A and B are constants for a particular gas and FFV is the fractional free volume defined as follows: FFV = (V-Vo)/V. The fractional free volume can be theoretically estimated from the molecular structure with the aid of the compass force field theory [19].

Ttypes of gas separation membranes

Membranes have been used as a separation technique since 1748 when Abbe Nollet experimented with a pig's bladder to separate water from the wine [34]. After establishing the concept of membrane separation, Thomas Graham completed the first experiment in 1829 for gas separation using a rubber polymer membrane [61]. With the revolution of industry and the demand of the fuel and energy, the importance of gas separation was

especially increased. As a result scientists began to search for a suitable material to be used as a membrane in an attempt to improve efficiency.

Depending on the material used, gas separation membranes can be divided into four categories: inorganic, mixed matrix, facilitated- diffusion, and polymeric membranes [36].

The concept of facilitated transport membranes is to ease the diffusion of the designated component by creating a bond between the gas molecule and the membrane [36]. This method has drawbacks such as mechanical instability, low diffusion rate, and formation flaws.

The inorganic membranes, although considered to be a good separating technique with thermal and chemical stability [62], are not favored in an industrial practice. This is due to the relatively high cost and complexity of handling and processing.

Unlike the previously mentioned inorganic membrane, polymeric membranes are considered to be a cost effective membrane with easy of handling and processing. Nevertheless, they lack both mechanical and chemical stability. Hence, their utilization is restricted to non-reactive and low temperature gases.

In order to improve polymer membrane shortcomings, blending of different polymers with different properties has been developed. Deriving a polymeric membrane by blending currently existing polymers instead of creating a new one is cost effective and time efficient [63]. At relatively high temperatures and pressures, such as those needed for natural gas purification, polymeric membrane performance may be hindered by CO_2

plasticization. To avoid this, polymers with resistance to plasticization [64] as well as enhanced thermal and mechanical properties [63] can be created via blending.

Mixed matrix membranes are a hybrid of inorganic and polymeric membranes capable of achieving the advantages of both membrane types. This membrane has outstanding gas separation behavior while maintaining mechanical and thermal stability. It is a cost effective technique with easy handling and processing [62].

Polymer membrane

In the early 80's, Permea [65] started to use synthesized polymers such as polysulfone hollow fibers to separate H_2/N_2. In early the 90's new types of polymer membranes were established in the market such as polyimide hollow fibers to separate CO_2/CH_4 [61].

After this many researcher used different types of polymers for gas separation such as poly(trimethylsilyl-1-propyne) [66], polybenzoxazoles [67], poly(diphenylacetylene) [68], polysulfone [69] and polyimide [21].

Choosing the proper material for a membrane is not easy because it has to balance the permeability and selectivity. Some reports [47] showed that rubbery polymers have high permeability and low selectivity and the author explained this result according to the loose chain packing [47]. On the other hand, glassy polymers showed low permeability and a significantly high selectivity when compared to rubbery polymers [70]. In order to use them in industrial applications, however, it has to be on a large scale [64].

Table 1: Recent publications of polymaric membranes used in gas separation.

Authors	Polymer	Modification	Remark	Application	Year
Basu et al. [71]	Polyimide	Metalorganic frameworks: $[Cu_3(BTC)_2]$, ZIF-8, MIL-53 (Al)	Selectivity and permeance of CO_2/CH_4 and CO_2/N_2 feeds under different CO_2 compositions simultaneously increased with higher filler loading.	CO_2/CH_4, CO_2/N_2	2011
Sakaguchi et al. [68]	Poly(diphenylacetylene)	Modified with nitric acid	The amination of poly(diphenylacetylene)s increased CO2 perm- selectivity and decreased gas permeability except	CO_2	2014
Goryaev et al. [72]	Poly(ethylene glycols)	Added ionic liquids	Increase in their permeability to CO_2	CO_2, O_2, N_2, and H_2	2014

Eguchi et al. [18]	Cross-linkable polyimide membranes	Enhanced transport plasticization resistance	Excellent balance of selectivity, permeability, and plasticization resistance.	CO_2 from CH_4	2015
Borjigin et al. [67]	Polybenzoxazoles	Thermally rearranged	The permeability coefficients of polymers significantly improved	CO_2	2015
Zhuang et al. [21]	Polyimide	Incorporating Tröger's Base	The incorporation of TB units into the PI backbone improved the gas transport performance	CO_2	2016

Developments of polymer membranes

Polymeric membrane advantages such as low cost of operation and ease of preparation and processing cause a huge spread of its use as a gas separation technology. On the other hand, polymeric membrane limitations such as low thermal and chemical stability cause problems such as plasticization at specific operation conditions. This makes it unreliable for use as a gas separation application in industry [3]. In order to avoid the polymeric membrane problems and improve performance, numerous methods have been suggested that include: crosslinking [73], copolymerization [74], polymer blending [75], thermal rearrangement [76], grafting of backbone, dual-layer hollow-fiber spinning [77], using fillers, i.e. mixed matrix membranes.

1.1.7 Mixed matrix membranes

Many studies suggest the production of mixed matrix membranes as a way to avoid the problem of inorganic and polymeric membrane [22], [78–81]. Mixed matrix membranes are simply a polymer matrix containing dispersed filler of inorganic material. Table 3 provides some of the recent work on improving the mixed matrix membranes in order to reach the needed selectivity and permeability.

Table 2: Some recent polymer blend membranes used in gas separation

Authors	**Polymer**	**Remark**	**Application**	**Year**
Mannan et al. [82]	Polysulfone(PSF) Poly(ether sulfone) (PES)	The addition of PES in the PSF membranes enhanced the separation performance of the blend membranes and, consequently, a 65% increment in the selectivity was observed in the PSF/PES membranes	CO_2 from CH_4	2015
Ahmad et al. [83]	Poly- benzimidazole (PBI) Polyvinylidene fluoride (PVDF)		67 % of the CO_2 in a gas mixture of H_2 and CO_2 could be removed	2015

Rabiee et al. [84]	Poly(ether-b-amide6)/ Poly(tetramethylene ether) glycol	Permeation results showed an increment in the tested gases along with enhancement in CO_2/H_2 permselectivity. However, CO_2/N_2 and CO_2/CH_4. permselectivity did not improve	CO_2 separation from H_2, N_2 and CH_4	2015
Giel et al. [85]	Polyaniline Polybenzimidazole	The permeability, diffusion and solubility coefficients decrease with increasing concentration of PANI in the blend. The ideal selectivity increase with increasing concentration of PANI in the blend	H_2,O_2,CH_4,N_2, CO_2 and water vapor	2016

Table 3: Recent publications about polymer nanocomposites for gas separation.

Researcher	polymer	Molecular sieve	Application	Remarks	Year
Dorosti et al.[86]	polysulfone/polyimide	zeolite ZSM-5	N_2, O_2, CO_2 and CH_4	The blend show higher permeability and acceptable selectivity in comparison with plain membranes	2011
Karkhanechi et al.[87]	Polyimide (PI)	Nano-zeolites 13X and 4A	N2,CH4,CO2,CO2/N2, CO2/CH4	Permeability is decreased and selectivity increased	2012
Magueijo et al.[88]	Polysulfone	Microporous carbon xerogels	CO2/N2 CO2/CH4, CH4/N2	higher selectivity	2013
Liang et al.[89]x	Polybenzimidazole Polyimide	ionic liquids [C4mim] [NTf2]	H_2,N_2, CO, CO_2 and CH_4	PBI membranes had high H2 selectivity to other gases, and [C4mim] [NTf2] improved gas permeabilities especially CO_2.CO_2, CO, H_2, N_2 and CH_4.	2014
Xiang et al.[90]	Layers of polyethylenimine (PEI) and poly(acrylic acid) (PAA)	montmorillonite (MMT) clay	O_2 barrier	Increasing the Diameter of Clays and Exposure Times increasing the permeability.	2014

Moghadassi et al.[91]	Polyvinylchloride Styrene-Butadiene-Rubber	Zeolite	He, N_2,CH_4,CO_2	permeability was increased and (CO_2/N_2), (CO_2/CH_4) and (N_2/CH_4) selectivities all were decreased by the increase of zeolite loading ratio	2014
KARĞIL[80]	Polyethersulfone, Polyimide	Zeolitic Imıdazolate Framework-8 (ZIF-8)	H_2/CO_2, CO_2/CH_4, H_2/CH_4	The permeability of all gases increased as the amount of the PI in the blend increased. Selectivity values increased with increasing PI composition.	2015

Fillers can be inorganic material such as zeolite [86], silica [93], metal oxides, and carbon molecular sieving [78]. However, these fillers have some limitations such as segregation, poor polymer-filler bonding and pore blocking, which make them undesirable for industrial applications. Zeolite is the most common filler among those listed and it has been studied by many researchers [86, 69, 38, 94] .

Layered silicates have attracted the attention of researchers because it shows a significant improvement in the polymer properties when compared to the pure polymer. Studies show that layered silicates can improve the tensile strength and heat resistance as well as decrease gas permeability and flammability [16, 26, 28, 95].

Role of clay

In polymer/clay composites the clay is present in a discontinuous phase while the polymer matrix is a continuous phase [96]. Adding clay to a polymer enhances the mechanical [14], [97–99], thermal [100–102], and barrier [103] properties as well as reduces the flammability [104] compared to the polymer alone. The enhanced properties are due to the nanoparticles dispersion inside the polymer matrix that can reinforce the structure and create diffusion obstacles for gas molecules [23]. Clay is a layered silicate material that enhances gas barrier properties when it is fully exfoliated in a polymer matrix [105]. Montmorillonite (MMT), one of the most studied clays [106–108], is an inorganic phyllosilicate composed of one inner alumina or magnesia octahedral layer sandwiched by two silica tetrahedral layers (Figure 3 [27]).

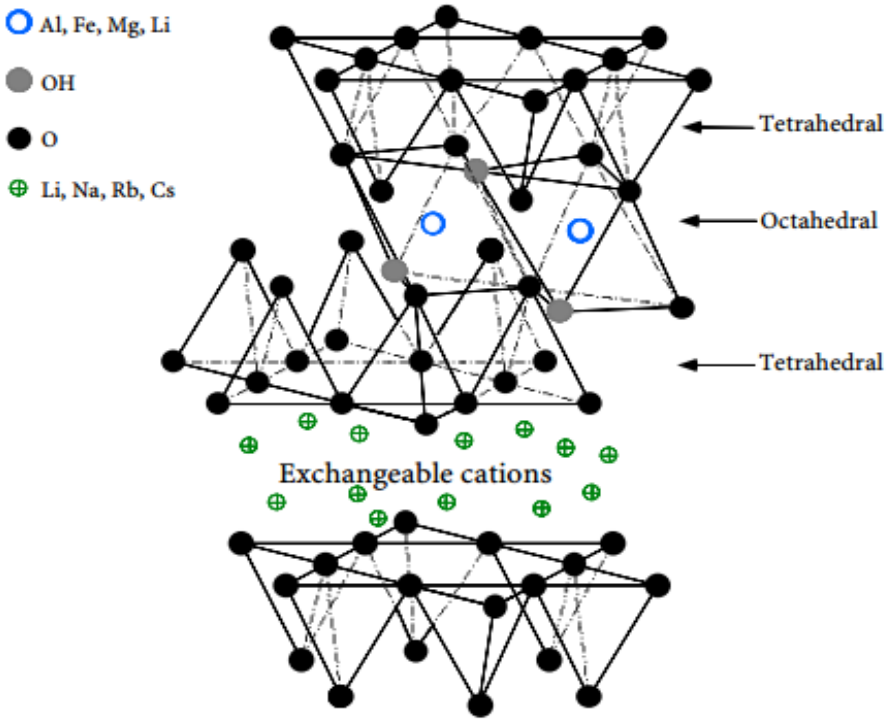

Figure 3: Montmorillonite clay chemistry and structure [27].

The most commonly used theory to explain the enhanced gas barrier characteristic of polymer/clay nanocomposites is Nielson's theory that was developed in 1967. This model focuses on the effect of the exfoliated clay to create a tortuous path for permeating molecules [109], as represented in Figure 4. The extension of the tortuous path will decrease the permeability of gas [110]. The increase in path length is a result of the high aspect ratios of the clay filler and volume fraction of the filler in the composite [111]. Permeabilities of different gases decreased when MMT was used as a filler in polyolefins [112], epoxy [113], polyamide [114], and polyurethane [8].

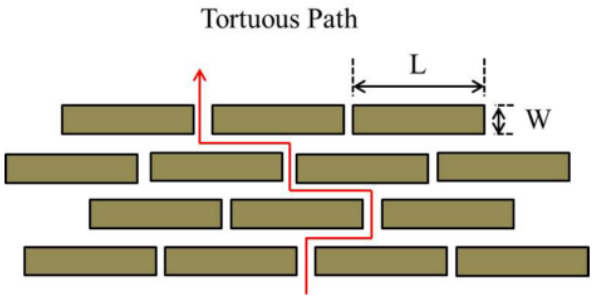

Figure 4 : Gas transport through a polymer-platelet composite via a tortuous path

Another benefit of the clay is that it works as a compatibilizer for the two polymers. Blending two or more polymers presents a way of creating an interesting mixture in properties that may not be present in a single kind of polymer. Nevertheless, resulting polymer blends usually have poor mechanical properties due to the unstable phase morphology formed during melt processing. Another unfavorable feature that is often present in polymer blends is thermodynamic immiscibility [115–117]. This behavior occurs as the entropy of mixing between segments of different polymers is not high enough to reach the required driving force for miscibility [118]. Regardless of this fact, there are a numbers of polymer-polymer pairs that offer valuable properties for different commercial products.

Other factors that may contribute to the incompatibility between mixed polymers are low interfacial adhesion, nonpolarity, and difference in molecular weight of the mixed polymers. Several studies have reviewed the thermodynamics of polymer blends [119, 120].

Monticelli et al. [121] studied the relationship between porous membranes and dense films formed from polysulfone mixed with three different types of clay: Cloisite Na, Cloisite 93A, and Cloisite 30B. Monticelli and her team used SEM to characterize the morphology of the composite and the results show that the clay dispersion was dependent on the type of clay. As noticed in the Figure 5, homogeneous dispersions of Cloisite Na and 93A aggregates were clearly observed, while no aggregates were present in the composite membrane prepared from Cloisite 30B.

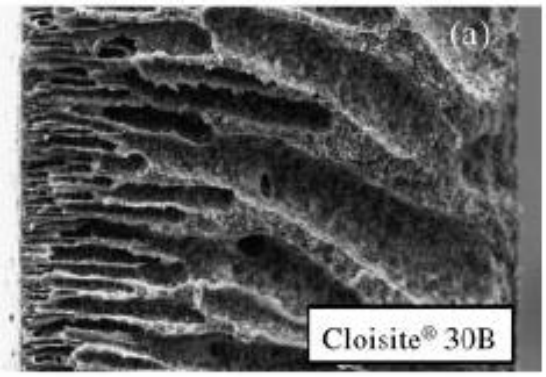

Figure 5: SEM results of polysulfone/30B membrane cross sections with 2% clay by secondary-electron emission [121].

Different studies have shown that there are significant improvements in permeability reduction to gases, moisture and organic vapors results when low concentrations of clay nanoparticles are added to various glassy polymers matrices [25],[6].

CHAPTER 3

3. EXPERMINTAL

3.1 MATERIALS

3.1.1 Polysulfone

Polysulfone was supplied by Solvay as Udel® P-1700 with a molecular weight of 56,600 (g/mol). Polysulfone has significant physical and chemical properties such as rigidity, toughness, and high-strength, making it a suitable thermoplastic material for continuous use up to 300 °F (149 °C). Furthermore, it is resistant to oxidation and hydrolysis. “Udel P-1700 polysulfone is highly resistant to mineral acids, alkali and salt solutions. Its resistance to detergents and hydrocarbon oils is good, but the resin may be attacked by polar solvents such as ketones, chlorinated hydrocarbons and aromatic hydrocarbons [122].

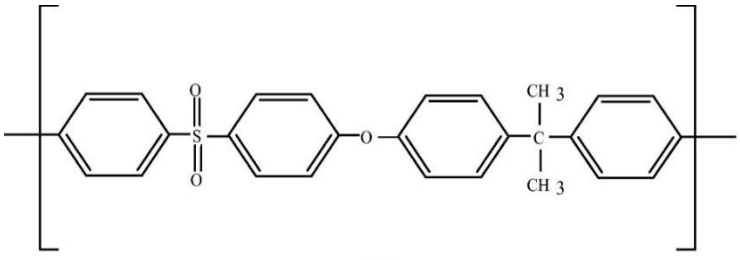

Figure 6: Structure of P-1700 polysulfone (PSU) [123]

3.1.2 Polyimide

Matrimid 5218 polyimide was supplied Alfa Aesar. It comes in the form of a yellow powder and has a density at 20 °C of 1.2 g/cm^3 and a melting point > 300 °C.

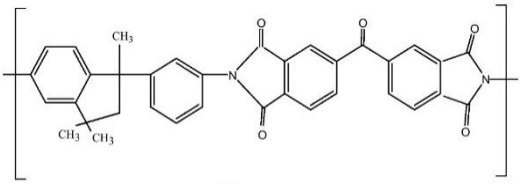

Figure 7: Structure of polyimide [123]

3.1.3 Solvent

N-dimethyl formamide (NMP) with a 99.1 g/mol molecular weight has been chosen as a solvent for its compatibility with both polyimide and polysulfone. The solvent was obtained from Aldrich Chemicals, and has a boiling point of approximately 180 ºC, liquid density at 20, 40 and 60 °C of 1.03, 1.02 and 0.99 g/ml, respectively. Its boiling point at 760 mm Hg is 204.3 °C.

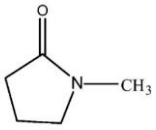

Figure 8**:** NMP solvent structure [123]

3.1.4 Clay

Cloisite® 30B was supplied by Southern Clay Products, and is a natural montmorillonite modified with a quaternary ammonium salt.

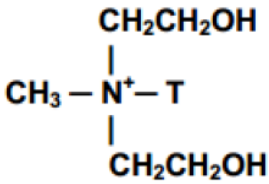

Figure 9: Structure of Colisite 30B. Ref. of this picture from Southern Clay website

3.2 Methods

Preparation of the polymer/clay films was done in three main steps: mixing, casting and drying.

3.2.1 Mixing

Mixing was done using a Thinky Mixer to mix the solvent with the polymer and clay. Figure 10 shows how the solution container revolves and rotates in a rotating-revolving manner at high speeds.

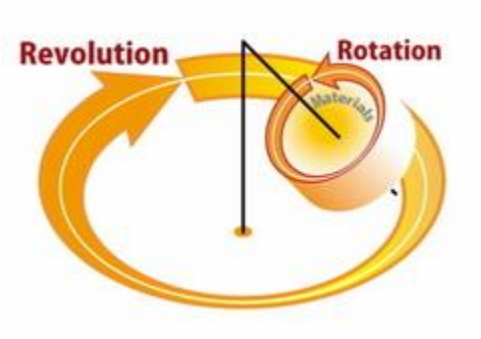

Figure 10: The mechanism of thinky mixer

(http://www.thinkyusa.com/commentary/jiten-kouten.html)

Polysulfone and polyimide with various loadings of cloisite 30B clay (0, 0.5, 1, 2 and 3%) were mixed with NMP solvent to obtain a 20 wt. % solution.

3.2.2 Solution casting

After preparing the polymer/clay mixture, solutions were cast on a sheet of glass using a Dr. Blade (Figure 11). Polysulfone/clay-NMP and polyimide/clay-NMP systems were created using five different clay loadings: 0, 0.5, 1, 2 and 3% C30B. The doctor blade gap was set as 200 and 559 μm, which results in approximately 40 and 70 μm thick films respectively after using two different methods for drying that depended on the corresponding mass fraction ratios of the solutions. The carrier speed was set to 10 cm/min for uniform casting conditions.

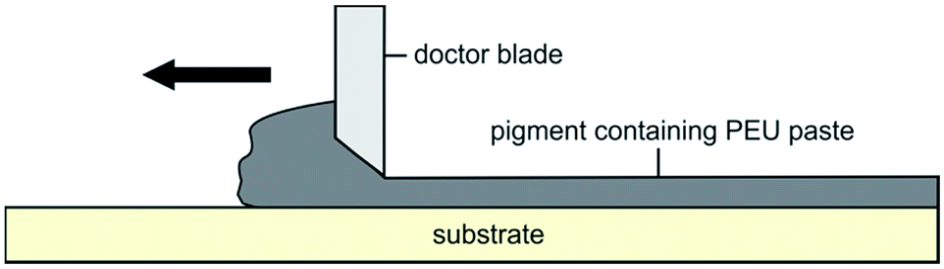

Figure 11: Schematic for Dr. Blade castig

3.2.3 Drying

The samples were placed in an oven at 120 °C for 2 hours after casting.

3.3 Characterizations

3.3.1 XRD

X-ray analysis was done on the PSF/Cloisite 30B and PI/Cloisite30B nanocomposite films to determine the level of polymer intercalation into the nanoclay layers. The intercalation of polymer(s) in between the nanoclay layers results in an increased interlayer distance. X-ray analysis is used to confirm this due to the cyclic arrangement of the silicate layers in both the pristine and intercalated states. X-rays are created when high energy electrons hit a metal target. A given wavelength (λ) for X-rays is diffracted via a system of parallel and equally distant lattice planes of spacing d_{hkl} that satisfies Bragg's Law (Figure 12).

$$n\lambda = 2d_{hkl} \sin\theta \qquad \text{Equation [4]}$$

where, n is a positive integer and denotes the order of reflection, λ is the wavelength, θ is the angle between the incident ray and the reflecting plane and d_{hkl} is the distance between the adjacent planes in the crystals.

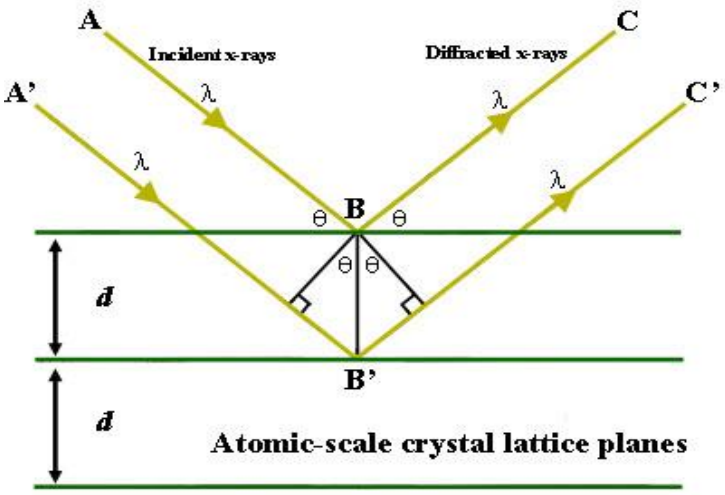

Figure 12: Bragg's law derivation. (http://www.eserc.stonybrook.edu/projectjava/bragg/)

Using wide angle X-ray scattering we investigated the distance between clay platelets for different loadings of nanocomposites. Experiments were performed in an X-ray diffractometer, Rigaku MiniFlexII (Figure 13). The electron source was Cu-Kα (λ=1.5404 Å). The instrument used ICDD (International Center for Diffraction Data) software to operate. The operation power is 50 kV and 20 mA. Scans were obtained in a 2θ range from 1.9° to 40°, with a 0.1° step size.

Figure 13: Miniflex Desktop X-ray diffractometer (XRD)

3.3.2 Gas barrier

Oxygen transsmision rate testing was performed by MOCON OX-TRAN® (Figure 14) in accordance with ASTM D3985-81 and ASTM F1249-01 using an Oxtran 2/21 ML instrument at 25 °C, 1 atm oxygen pressure and 0% relative humidity. This device uses a continuous flow method (ASTM D3985-81 and ASTM F1249-01) along with nitrogen as the carrier gas in order to measure oxygen flux, J(t), through the composite membrane. The membrane samples were carefully conditioned in the device, as described in a previous

study [124]. The steady state flux j_∞ was used to calculate the permeability coefficient (P) by using Equation 5 .

$$P = \frac{j_\infty x l}{\Delta p} \qquad \text{Equation [5]}$$

where l is the film thickness and Δp is the oxygen partial pressure difference across the membrane.

Figure 14: OX-TRAN® (MOCON).

Dielectric spectroscopy

Dielectric spectra were isothermally measured via a Novocontrol GmbH Concept 40 Broadband Dielectric Spectrometer (BDS) (Figure 15) within the temperature range of -80 to 250 °C and frequency range 0.1 Hz - 3 MHz. Samples were stored in a desiccator at

room temperature for approximately one week before BDS experiments were performed to reduce the obscuring effect of water on the dielectric readings. Each sample was covered on both sides with aluminum sheets and the assembled sample was placed in the middle of two stainless steel electrodes with a diameter of 2 cm. Finally, samples were placed in the instrument for data collection.

The Havriliak-Negami (H-N) equation [122-124] was used to fit the experimental data in order to obtain the important information on each relaxation process in the composite especially after the insertion of clay:

$$\varepsilon^*(\omega) = \varepsilon' - i\varepsilon'' = -i\left(\frac{\sigma_{dc}}{\varepsilon_0 \omega}\right)^N + \sum_{k=1}^{3}\left[\frac{\Delta\varepsilon_k}{\left(1+\left(i\omega\tau_{HN}\right)^{a_k}\right)^{b_k}} + \varepsilon_{\infty k}\right] \qquad \text{Equation [6]}$$

where ε′ represents real dielectric permittivities and ε'' represents imaginary dielectric permittivities, where i equals √-1. The sum contains three relaxation terms while the left term is related to the DC conductivity. ε_0 represents vacuum permittivity, ω represents $2\pi f$, and σ_{dc} represents DC conductivity. "For each relaxation term *k*, the dielectric strength $\Delta\varepsilon_k = (\varepsilon_R - \varepsilon_\infty)_k$ is the change between ε' at low and high frequencies, respectively." [128] The exponent *N* symbolizes conduction with regards to the nature of charge hopping pathways and mobility constraints [128] and *a* describes the breadth of asymmetry of the ε'' vs. ω peaks while *b* describes its degree. Havriliak-Negami relaxation time τ_{HN} is associated with the actual relaxation time (τ_{max}) at loss peak maximum (f_{max}) as illustrated in the following equation [129]:

$$\tau_{\max} = \tau_{HN}\left[\frac{\sin\left(\frac{\pi a b}{2(b+1)}\right)}{\sin\left(\frac{\pi a}{2(b+1)}\right)}\right]^{\frac{1}{a}} \qquad \text{Equation [7]}$$

In Equation 7, the DC term is attributed to the unintended or inherent charge migration that is usually deducted to reveal loss peaks or make them further distinctive.

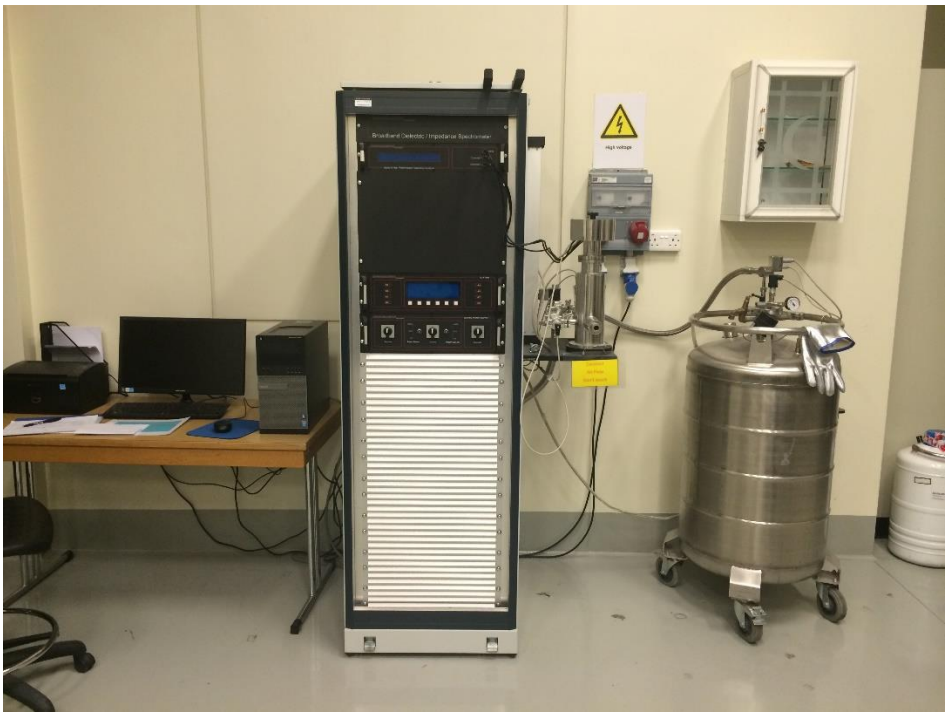

Figure 15 : Novocontrol GmbH Concept 40 broadband dielectric spectrometer.

CHAPTER 4

4. RESULTS AND DISCUSSION

In this work, two polymer-based nanocomposite systems have been prepared using a doctor blade casting technique. The results and discussion chapter is divided into three main sections: preparation of polymer nanocomposite films, as well as its optimization and characterization using SEM, EDX, and XRD (section I), dielectric studies via a broadband dielectric spectrometer to understand the homogeneity of samples, chain motion dynamics, and interfacial interactions (section II), and investigation of enhanced gas barrier property performance for gas separation applications (section III).

4.1 Morphology And Structural Properties

The morphology and structure properties could be found by different characterization methods, such as, X-Ray Diffraction (XRD) , scanning electron microscope (SEM), and EDX.

4.1.1 X-ray diffraction (XRD)

X-ray diffraction analysis was done on the PSF/Clay and PI/Clay nanocomposite films to determine the level of polymer exfoliation into the nanoclay layers. The exfoliation of polymer in between the nanoclay layers results in an increased interlayer distance, and this nanocomposite structure is commonly monitored with XRD where the clay diffraction peaks are observed to disappear due to the crystallographic order being lost when completely exfoliated [130]. As such, XRD is particularly studied for this purpose, due to the cyclic arrangement of the silicate layers in both the pristine and exfoliation states. Wide-angle X-ray diffraction measurements of the Cloisite® 30B powder and the PSF/Cloisite® 30B nanocomposite membranes are shown in Figure 16. Patterns show that the pure Cloisite 30B has a characteristic peak at $2\theta = 4.7°$ which is attributed to the basal spacing (~ 20.8 Å). It is noticed that the main peak of the clay disappeared, which indicates a high degree of exfoliation.

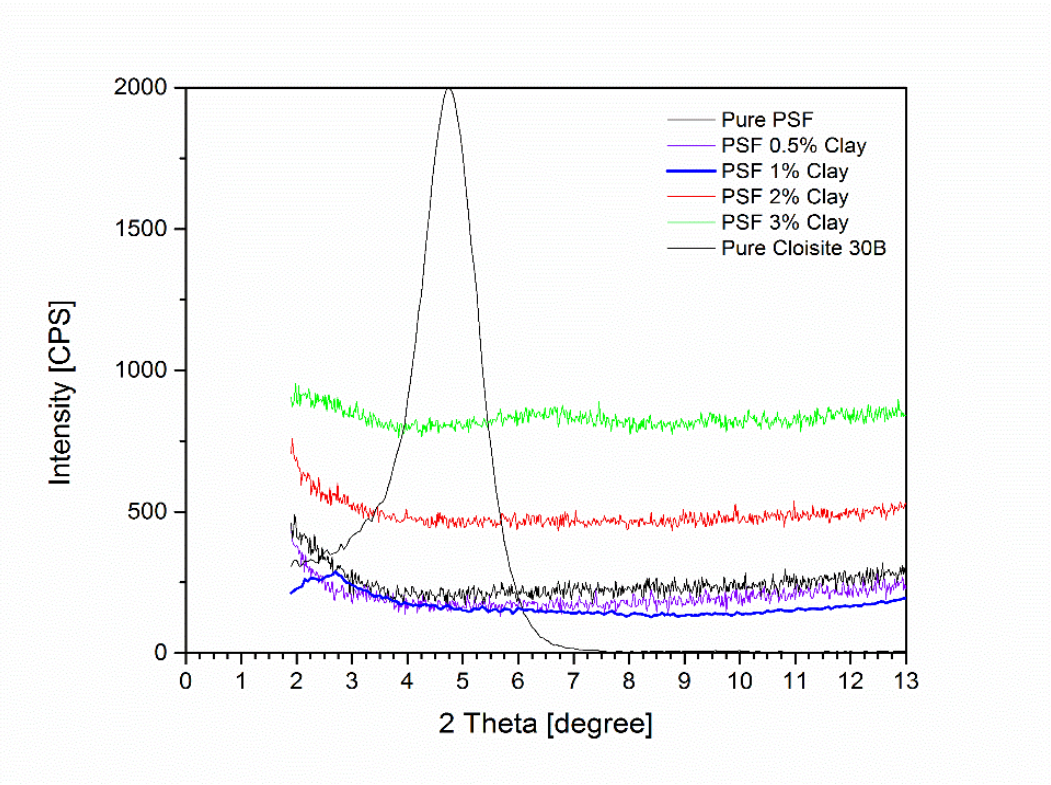

Figure 16 : X-ray for neat PSF and different C30B loading nanocomposite films

The XRD patterns of the Cloisite® 30B powder and the PI/Cloisite® 30B nanocomposite membranes are presented in Figure 17. The observed dip in the interplanar spacing of the PI/Cloisite® 30B sample at a loading of 0.5,1 and 2 wt% have completely disappeared, which reveals the formation of exfoliated structures due to the interactions between the PI network and clay platelets. On the other hand, a 3wt% clay loading shifts the peak to a lower 2θ position at approximately 2θ = 6.8° indicating a mixed morphology of the clay.

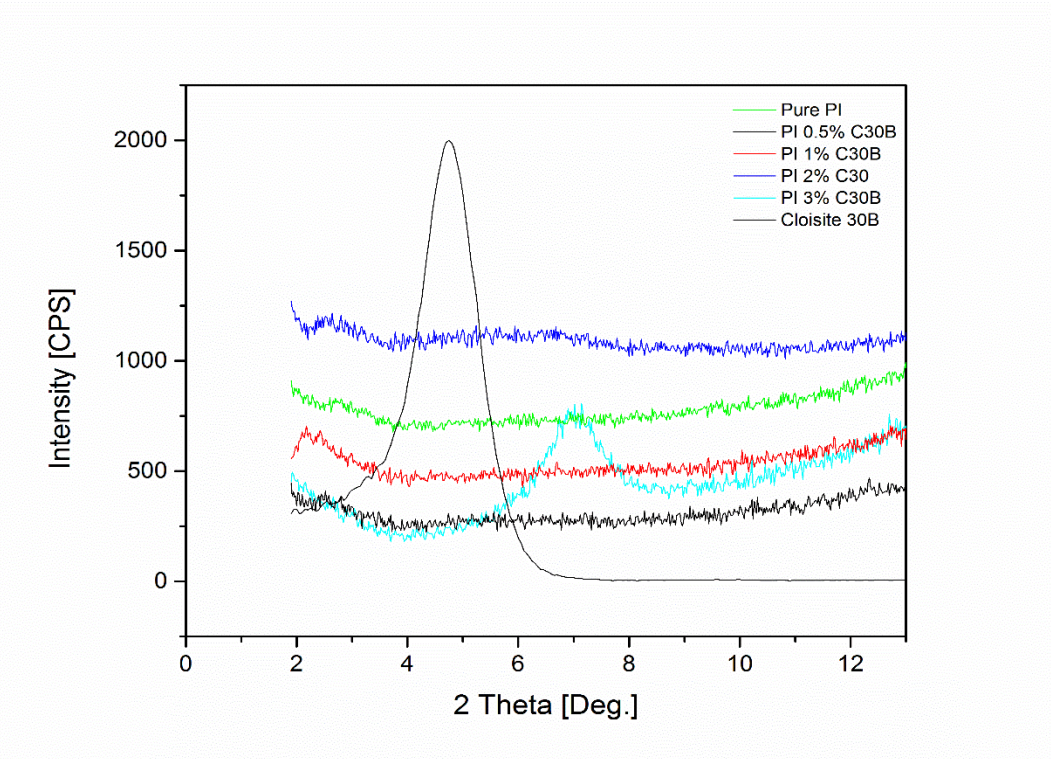

Figure 17: X-ray for neat PI and the C30B nanocomposite films. 2-theta in degrees

4.1.2 Scanning Electron Microscope (SEM), and EDX

The morphology of Cloisite 30B nanoparticles in PSF and PI was observed by scanning electron microscopy (SEM) of freeze-fractured specimens.

Figure 18 show a cross-sectional SEM image with analysis using energy dispersive x-ray (EDX), for both PI and PSF with 1% clay. The image show that the Cloisite 30B nanoparticles have uniform dispersion in the PSF and PI matrix as indicated by the red color of Cloisite 30B particles, which is mainly the silica element of Cloisite 30B. This well dispersion of clay also confirms in our previous result of XRD.

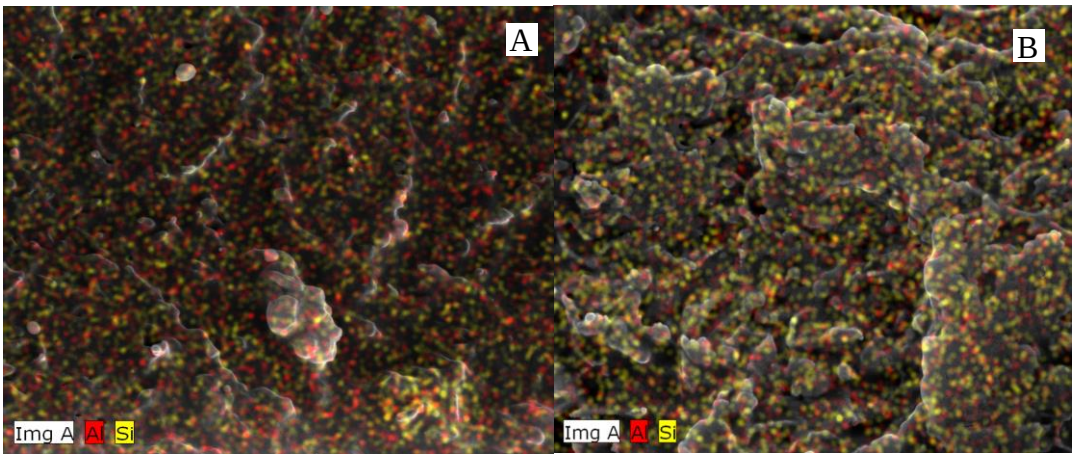

Figure 18: SEM and EDX mapping analysis shows the dispersion of 1% C30B nanocomposite in : (A) PSF film , (B) PI film.

5. DIELECTRIC STUDY

Modern broadband dielectric spectroscopy (BDS) is a powerful material characterization tool with strong capabilities for examination of polymer chain molecular dynamics over broad frequency (*f*) ranges, temperatures, distance and time scales [129]. For example, Mauritz and Hassan used BDS to characterize the glass transition temperatures [131] and chemical degradation in polylactides [132] and Nafion® membranes [133]. Besides polymer chain relaxations, changing interfacial polarization can be due to the alterations in dielectric permittivity and/or charge conductivity across phase margins [134].

Dielectric spectroscopy examines interactions of applied electric fields in alternating directions (AC field) with dipoles having reorientation mobility in materials. Long-range cooperative chain motion of segments, which is affected by glass transition, and dipole rearrangements are influenced by the conformational fluctuations on different distance scales.

In this study, we investigate the effect of clay on the dynamics of the glass transition temperature (T_g) and secondary relaxations of polysulfone and polyimide composites. Changes in these relaxations with addition of clay reflect changes in the free volume and physical aging, which ultimately affect membrane performance in gas separation applications.

Secondary Relaxations and Glass-rubber Transition in Polysulfone/Clay Composites

Figure 19 shows the different relaxation processes exhibited by the control polysulfone (PSF) sample before clay addition. Crests of the 3D dielectric permittivity loss (ε'') – frequency (f) - temperature (T) response surfaces over a broad range of temperatures (-80 to 250 °C) are displayed. Three types of relaxations are evident in Figure 19, namely, γ, β, and Tg-relaxations, respectively, in the order of their appearance from low to high temperature. A detailed analysis of these three relaxations and effect of clay addition on their motions will be the subject of the following section of this chapter.

The γ-relaxation is assigned to the local dipole oscillations of the $–SO_2$ and the $–(CH_3)_2$ groups of the sulfone (SU) and the bisphenol (BP) sides of the polymer, respectively [135], [136]. Other researchers ascribed this relaxation to fluctuations of the phenyl rings of the bisphenol [137] or the sulfone [138] sides or to a superposition of the local motion of the rings in both sides [139].

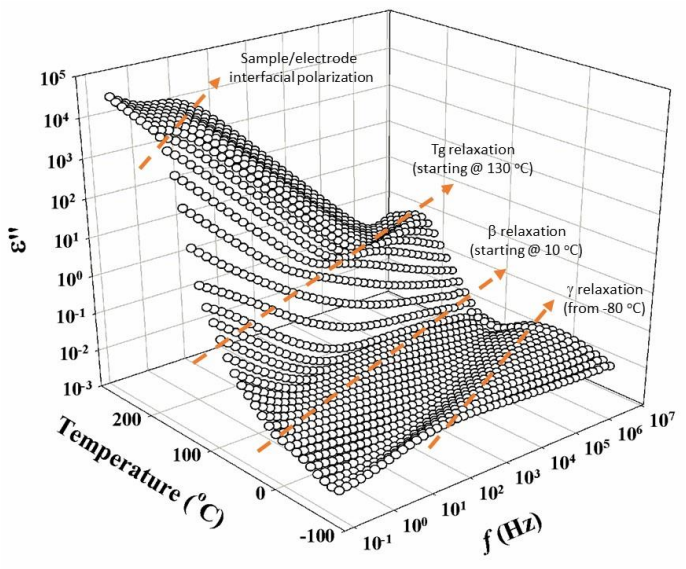

Figure 19 : $\varepsilon'' - f$ - T response surfaces for the control PSF sample. Curves are spaced at 10 °C increments and arrows follow the crests of different relaxations to show their progression with temperature.

More in-depth insight on the γ-relaxation is shown in the ε'' vs. frequency spectra as a function of temperature for different samples in Figure 20. Experimental data were fitted to the H-N equation (Eqn. 6) which displayed very good fits, as indicated by the solid lines.

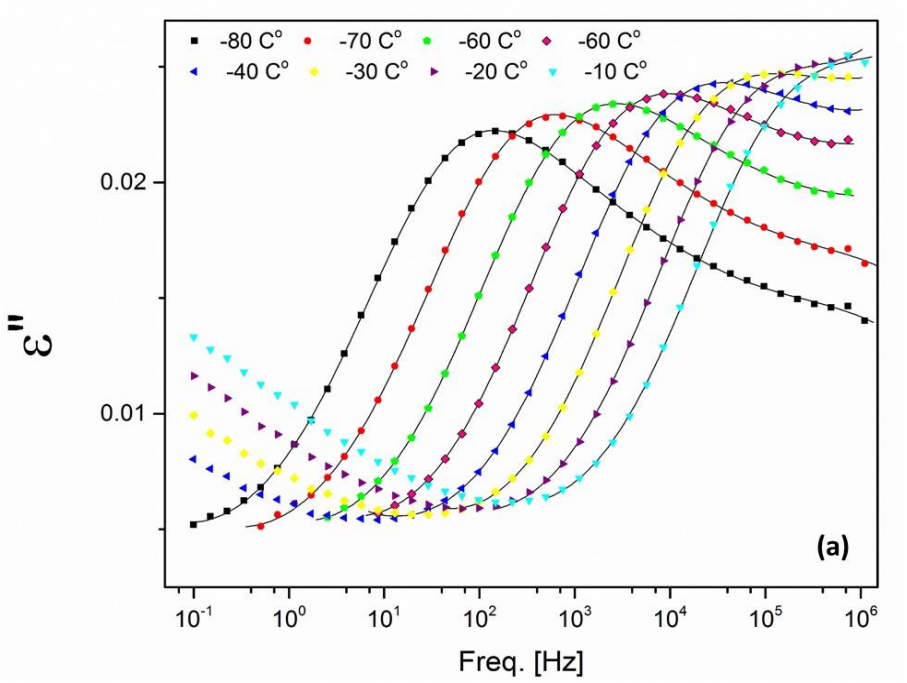
-80 C°
-70 C°
-60 C°
-60 C°
-40 C°
-30 C°
-20 C°
-10 C°
0.02
0.01
ε"
(a)
10^-1
10^0
10^1
10^2
10^3
10^4
10^5
10^6
Freq. [Hz]

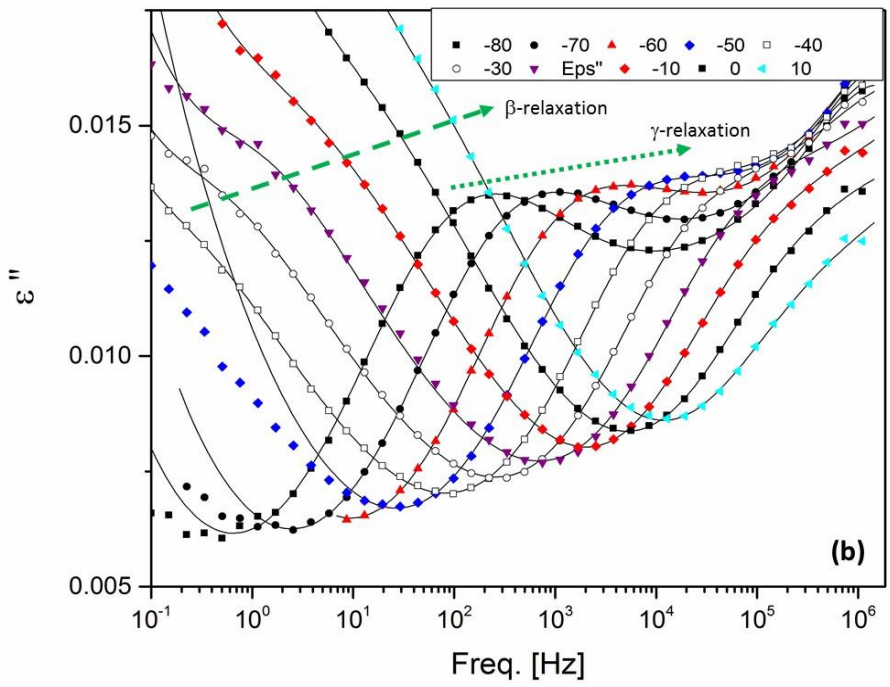
-80
-70
-60
-50
-40
-30
Eps"
-10
0
10
β-relaxation
γ-relaxation
0.015
0.010
0.005
ε"
(b)
10^-1
10^0
10^1
10^2
10^3
10^4
10^5
10^6
Freq. [Hz]

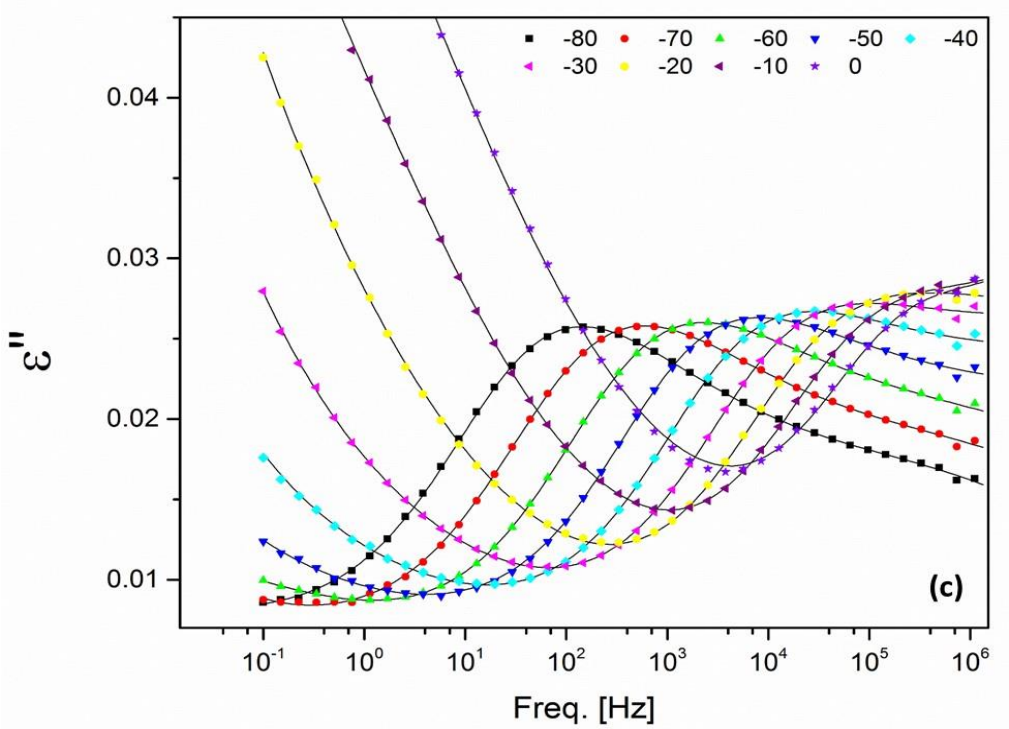

Figure 20 : Frequency dependence of the ε'' at different temperatures showing the γ-relaxation for the PSF control (a), 0.5wt% clay (b), and 3wt% clay (c) samples. Lines represent the H-N equation fits to the experimental data.

γ-relaxation peak maxima for the samples shift to higher frequency with increasing temperature, indicating faster local motions for the $–SO_2$ and $–(CH_3)_2$ dipoles, and therefore, shorter relaxation times. An interesting feature of Figure 24b is the presence of an additional relaxation at -30 ^oC which could account for the β-relaxation motion of the PSF. β-relaxation is of more cooperative nature than the γ-relaxation and accounts for intra- and interchain cooperative motion of several segments [136]. These motions are

related to packaging defects and should disappear after extended annealing [140], [141]. For the 0.5wt% clay sample, β-relaxation was observed at a much earlier temperature than the other samples (-30 ^{o}C vs. 10 ^{o}C for all other samples). This could be due to some slight difference in the annealing process during the preparation of the 0.5wt% clay sample as compared to the rest. Further investigation of this relaxation and its activation energy changes with clay loading is currently in progress.

Relaxation times ($\tau_{max} = 1/2\pi f_{max}$) of the γ-process motion were extracted at each temperature from the H-N model fits of the spectra in Figure 25. Plots of log τ_{max}vs. the reciprocal of temperature (1/*T*) revealed strong Arrhenius behavior according to the following equation:

$$\tau_{max}(T) = \tau_0 \exp\left(\frac{E_a}{RT}\right) \qquad \text{Equation [8]}$$

Where E_a is the activation energy, R is the universal gas constant and τ_o is a pre-exponential factor. Temperature dependence of the relaxation times in Figure 21 is linear, rather than WLF-like, indicating that the γ-relaxation related motions are local and less cooperative.

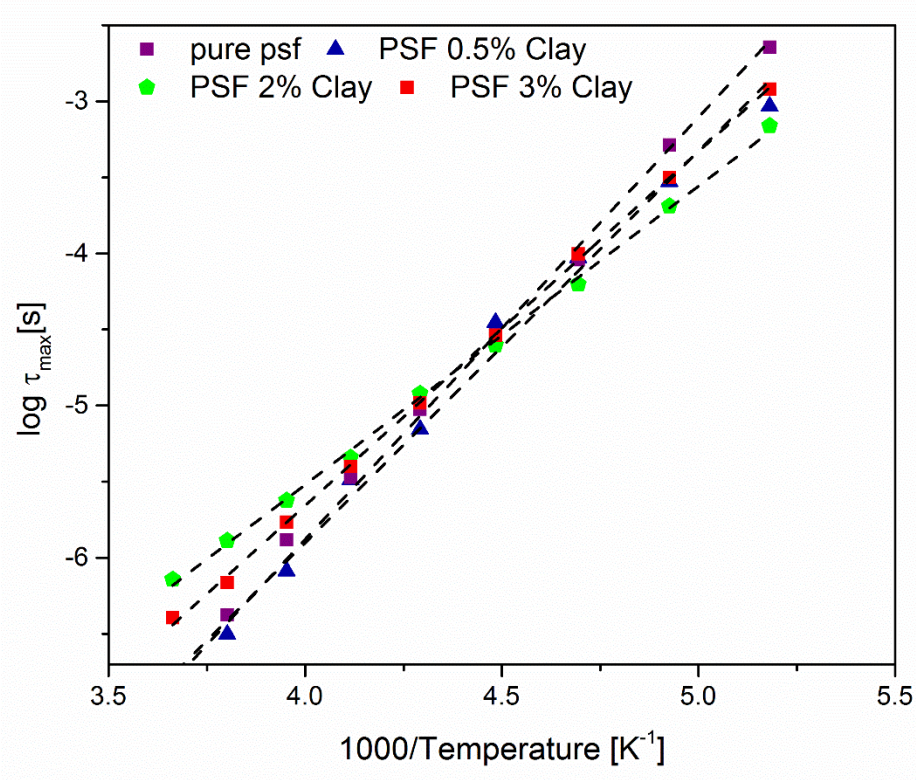

Figure 21 : Arrhenius plots for the γ-relaxation in the polysulfone composite samples. Lines represent the best fits to the data

Values of the activation energies for the γ-relaxation are calculated in Table 4. These values are within the typical range for secondary relaxations in glassy polymers. The activation energy values are observed to systematically decrease with increasing clay loading up to 2wt% clay in PSF. However, the activation energy increased with addition of 3wt% clay, suggesting that the high loading of clay could have introduced some packing

defects within the polysulfone rigid backbone,thereby facilitating the fluctuation motions of the $–SO_2$ and $–(CH_3)_2$ groups.

Table 4 : Calculated activation energies for the γ-relaxation in the polysulfone composite samples

Sample	Activation energy (kJ/mol)	Fit R^2
Pure PSF	53.03	0.9986
PSF 0.5 clay	49.22	0.9969
PSF 2%clay	37.51	0.9986
PSF 3%clay	44.48	0.9998

Figure 22 shows the ε'' vs. f spectra of the T_g-related relaxation for the PSF control and clay composites samples. The T_g-relaxation is associated with the T_g related motions and is assigned to long-range cooperative segmental fluctuations of polysulfone [135], [136]. All spectra seem to have a very good fit to the Havriliak-Negami (H-N) model (Eqn. 6), as clearly shown by the solid lines passing through the experimental data points. The linear monotonic raise of ε'' values at low f accounts for the DC-conduction due to the presence of unintended ionic impurities, which could be remaining from the polymer synthesis as well as those resulting from the addition of the clay. At low f, ion hopping events will have

enough time to be sampled during the experimental time scale of a half period of oscillation $(2f)^{-1}$ and before the applied electric field reverses. Above the T_g, ion hopping events will be even greater due to the increased chain segmental mobility,thus causing rapid increase in the ε'' values.

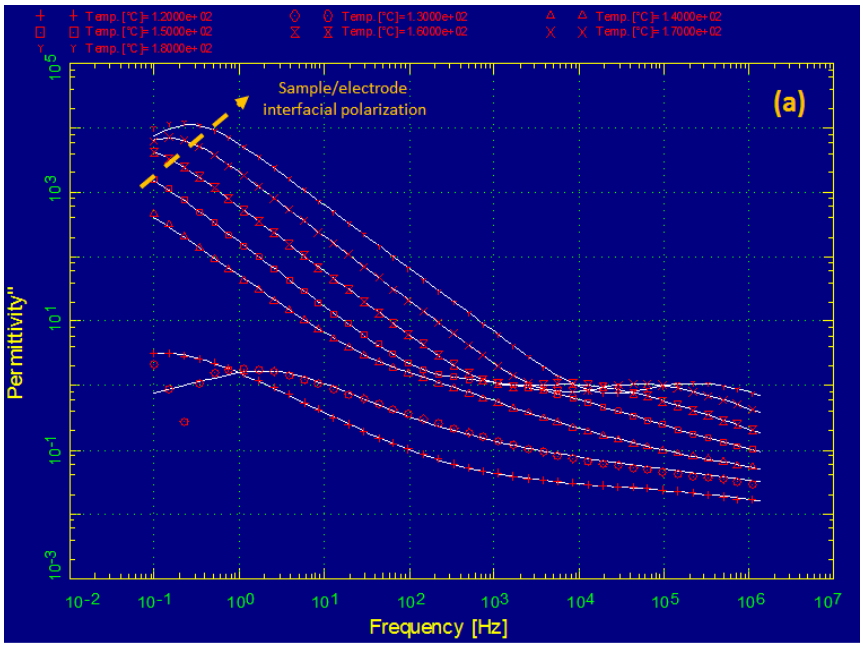

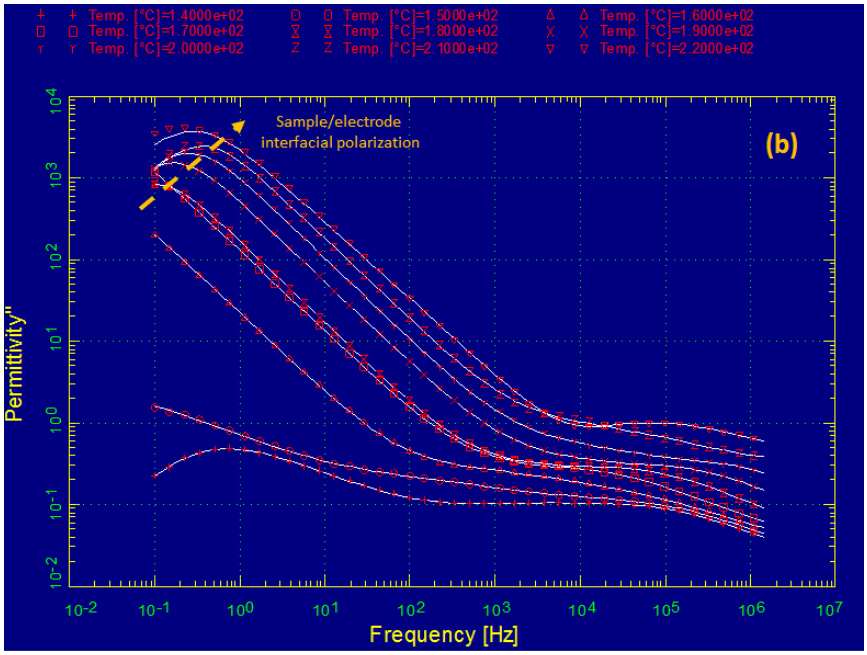
Temp. [°C]=1.4000e+02
Temp. [°C]=1.5000e+02
Temp. [°C]=1.6000e+02
Temp. [°C]=1.7000e+02
Temp. [°C]=1.8000e+02
Temp. [°C]=1.9000e+02
Temp. [°C]=2.0000e+02
Temp. [°C]=2.1000e+02
Temp. [°C]=2.2000e+02
Sample/electrode
interfacial polarization
(b)
Permittivity''
Frequency [Hz]

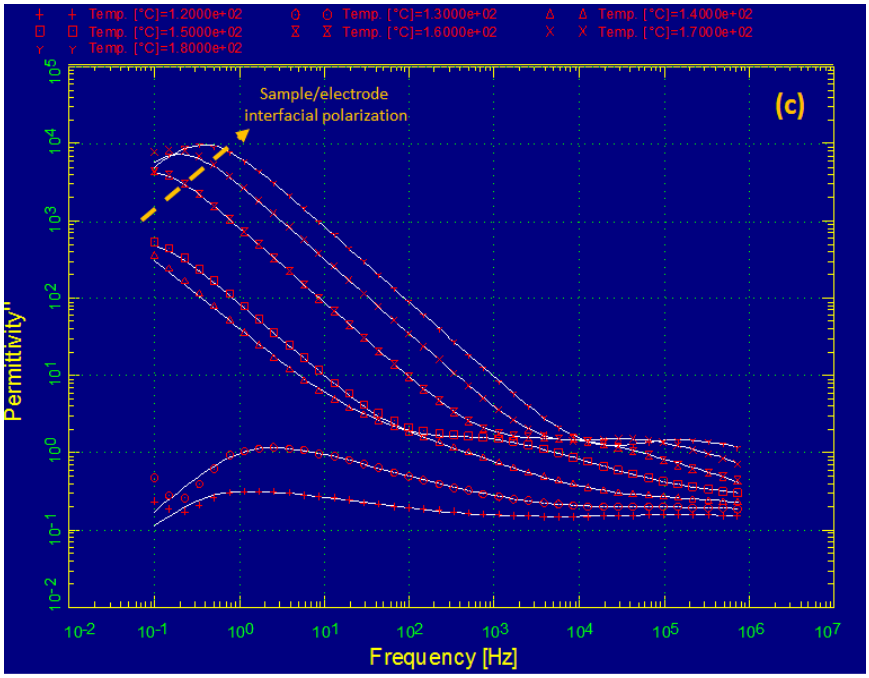
Temp. [°C]=1.2000e+02
Temp. [°C]=1.3000e+02
Temp. [°C]=1.4000e+02
Temp. [°C]=1.5000e+02
Temp. [°C]=1.6000e+02
Temp. [°C]=1.7000e+02
Temp. [°C]=1.8000e+02
Sample/electrode
interfacial polarization
(c)
Permittivity''
Frequency [Hz]

Figure 22 : Frequency dependence of the ε'' at different temperatures showing the T_g-relaxation for the PSF control (a), 0.5% clay (b), and 3% clay (c) samples. Lines represent the H-N equation fits to the experimental data.

Figure 22 also shows a signature of the sample/electrode interfacial polarization relaxation on the loss spectra indicated by the downward curvature of the ε" values approaching low f [142]–[144]. This phenomena is caused by rapid accumulation of charges in the near-electrode regions especially at faster segmental mobility when $T > T_g$.

As discussed earlier for the γ-relaxation, relaxation times corresponding to the ε″ vs. f peak maximum within the T_g region were obtained from fitting the H-N equation to the data. The Vogel-Fulcher-Tammann-Hesse (VFTH) equation [145], shown below, was then fitted to τ_{max} vs. T data:

$$\tau_{max}(T) = \tau_0 \exp\left(\frac{E_a}{k_B(T - T_V)}\right) \qquad \text{Equation [9]}$$

Where k_B is the Boltzmann constant and τ_0 is a hypothetical relaxation time at infinite temperature. E_a, while having units of energy but is not associated with an activated process in the common sense. T_V, the Vogel temperature, is the temperature at which chain segments become frozen in a supposed situation of cooling a polymer from the rubbery state in a quasi-static manner.

Figure 23 shows $\log_{10} \tau_{max}$ vs. T^{-1} plots for the PSF and its clay composite samples. The curvature (as opposed to linearity) of all plots is typical for the long-range motions in glass-forming polymers. The curves for the pure PSF and 3% clay samples are almost identical and are moderately down-shifted on the plot relative to the 0.5 and 2% clay samples. This down-shifting feature indicates that chain motions are faster in the case of pure PSF and 3% clay samples.

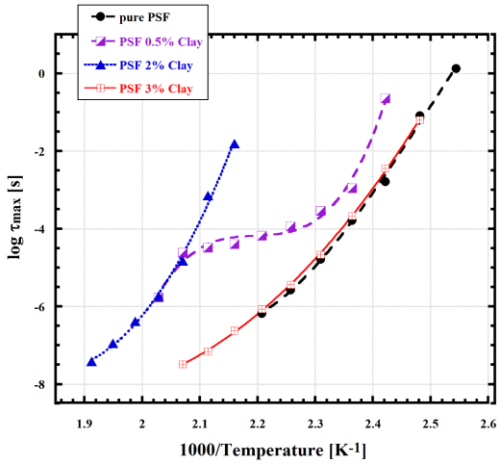

Figure 23 : . VFTH plots for the T_g-relaxation of the polysulfone/clay composite samples.

Vogel temperatures extracted from the VFTH equation fitting to the data are given in Table 5. As generally explained, higher T_v corresponds to more effective chain packing, i.e., lower free volume, in a hypothetical equilibrium-like state via quasi-static cooling. Based on this view, a lower specific volume for the 0.5 and 2% clay samples would suggest more

efficient chain packing and therefore a higher T_g relative to the pure PSF sample. This conclusion supports the decrease in O_2 permeability, reported above, with the addition of clay. While the reported results for the 3% sample may suggest higher free volume, this phenomena will require further investigation to explain it.

Table 5 : Calculated Tv values for the T_g-relaxation in the polysulfone composite samples.

Sample	T_v (K)
Pure PSF	295
PSF 0.5% Clay	320
PSF 2% Clay	396
PSF 3% Clay	239

Secondary Relaxations in Polyimide/Clay Composites

The material under investigation in this section is Matrimid®, which is an amorphous high T_g thermoplastic polyimide (PI). Matrimid is commonly used as gas separation membranes but one main challenge encountered is physical aging [146], [147]. The following analysis will use broadband dielectric spectroscopy to shed light on changes to secondary motions

with addition of clay in the PI/clay composites and the potential impact of these modifications to the physical aging phenomena. Physical aging is strongly linked to segmental mobility changes and shifts from equilibrium state [148]. Therefore, inclusion of clay would cause the sub-T_g motions to endure physical aging and allow it to proceed towards equilibrium with minimal localized rearrangements [149]. Understanding the effect of clay on secondary relaxations and its link to physical aging could ultimately result in the development of valuable strategies to control physical aging in these composite membranes and greatly enhance their performance during applications.

Figure 24 shows the secondary relaxation processes in the control polyimide (PI) sample before clay addition. Crests of the 3D ε''- f - T response surfaces over a temperature range of -80 to 250 °C are shown. Two relaxations are displayed in Figure 28: γ-relaxation in the low temperature region and β-relaxation at approximately 20 °C.

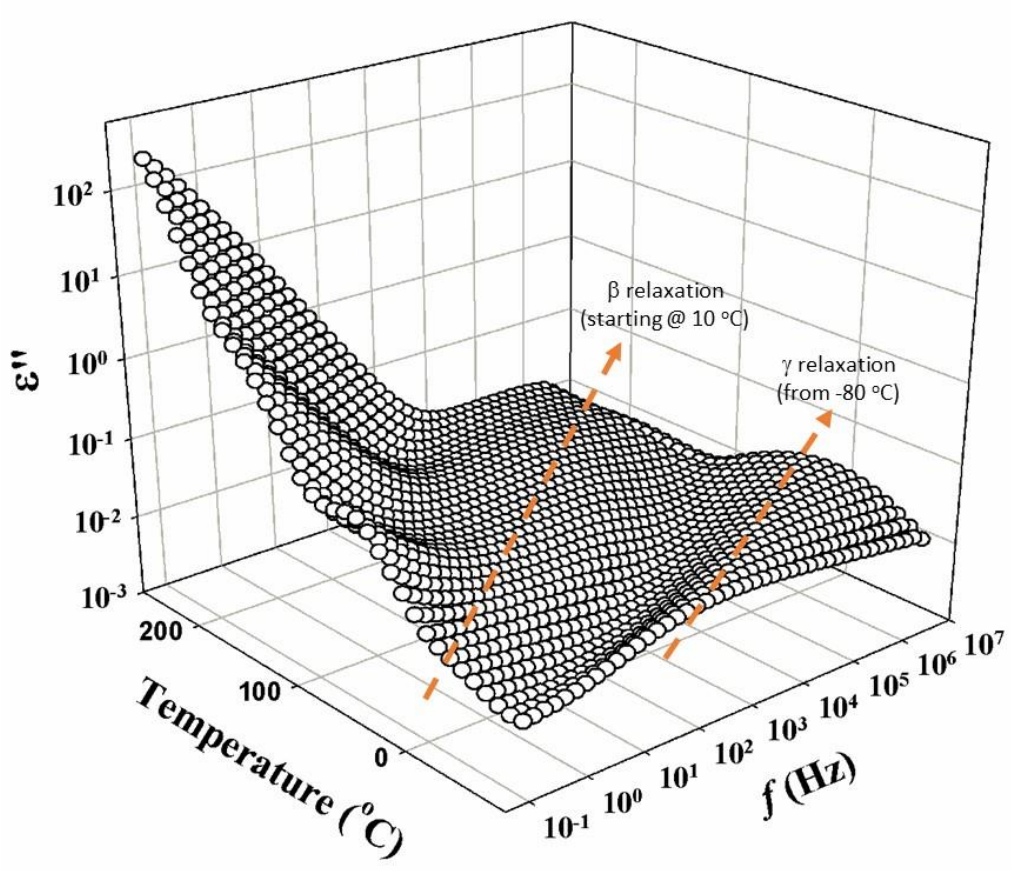

Figure 24: ε'' - f - T response surfaces for the control PI sample. Curves are spaced at 10° C increments and arrows follow the crests of different relaxations to show their progression with temperature.

The γ-relaxation is linked to localized motions involving phenyl ring oscillations as well as coupled water molecules[150]–[152], while the β-relaxation is assigned to local, short-range, cooperative motions that comprehend larger portions of the PI repeat unit [153] [154]. Some authors revealed that this relaxation would also include two components: β_1

which is associated with motions in the diamine section of the repeat unit and β_2 which is caused by motions of the dianhydride segment [155] [156].

Figure 25 depicts the temperature dependence of ε'' for the PI and its composite samples containing varying amounts of clay. With addition of clay, both β and γ-relaxation peak maxima shift to lower temperatures revealing more facilitated motions for the segments and moieties involved in these relaxations. This is possibly caused by increased free volume after the addition of clay.

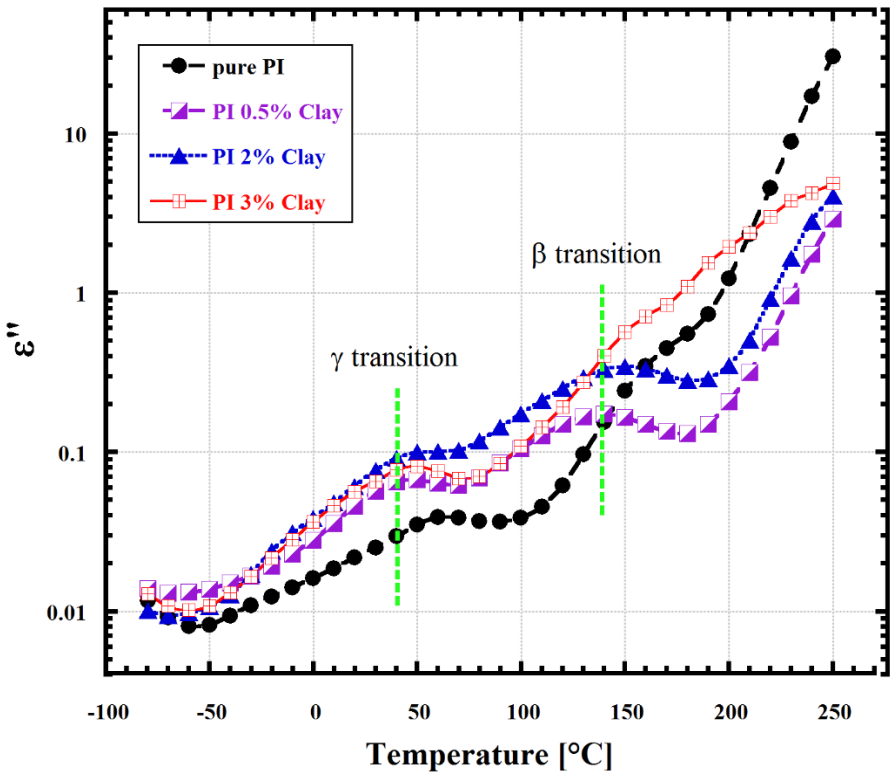

Figure 25: Temperature dependence of ε'' at 1 Hz for the PI/clay composites showing the γ and β-relaxations

The secondary relaxations in PI were fitted to the H-N equation (Eqn. 6) and the samples showed very good fits, as depicted by Figure 26.

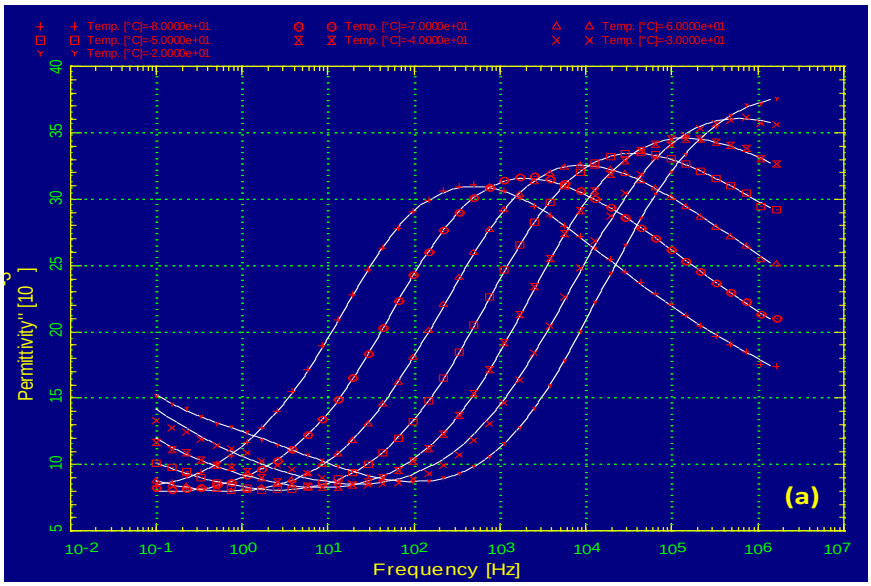

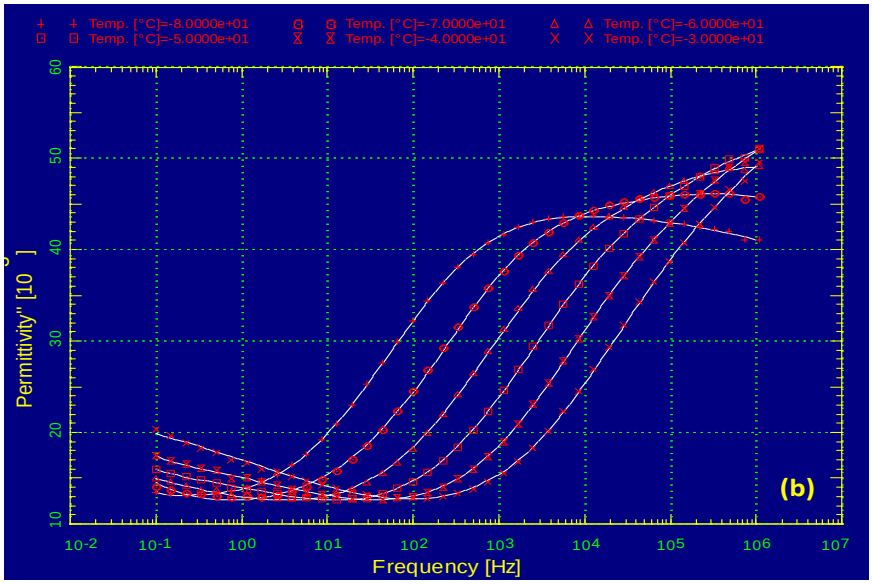

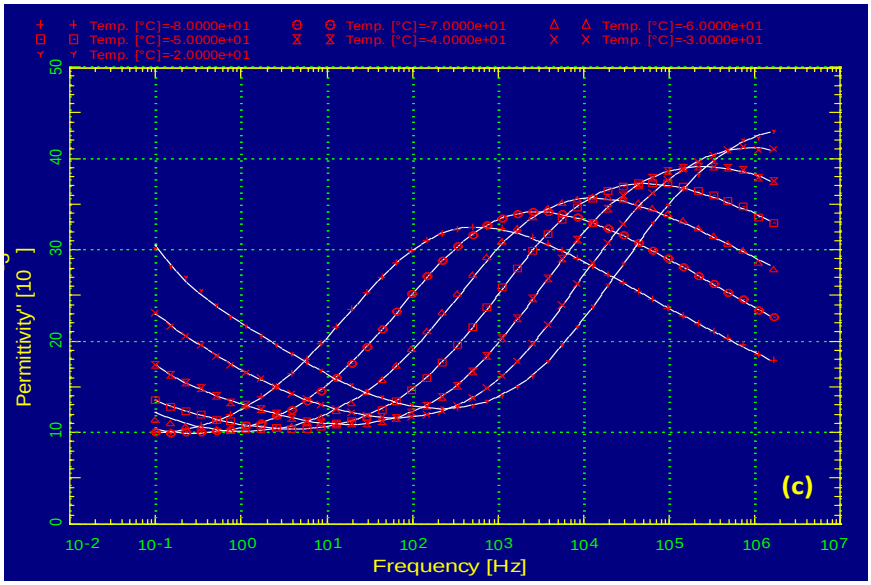

Figure 26: Frequency dependence of the ε'' at different temperatures showing the γ-relaxation for the PI control (a), 0.5% clay (b), and 3% clay (c) samples. Lines represent the H-N equation fits to the experimental data.

γ-relaxation peak maxima for the samples shift to higher frequency with increasing temperature, indicating faster phenyl ring oscillations. Less symmetric behaviour observed in the 0.5% clay sample might indicate a much broader distribution of relaxation times for this sample. This is in contrast to the control and the 3% clay samples which exhibit more symmetric and well-resolved peaks. Such behavior for the 0.5% clay sample might reflect different environment around the chains as compared to other samples.

Relaxation times ($\tau_{max} = 1/2\pi\ f_{max}$) of the γ-process motion were extracted at each temperature from the H-N model fits of the spectra in Figure 26. Plots of log τ_{max} vs. $1/T$ revealed an Arrhenius behavior in Figure 27, from which the activation energy values were calculated and presented in Table 6.

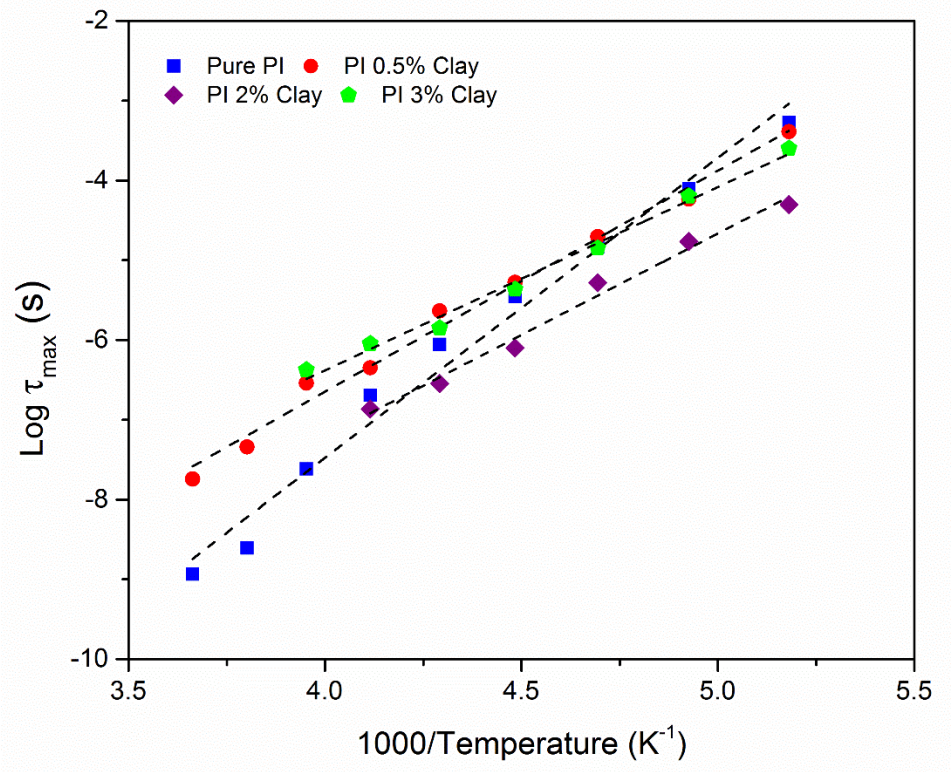

Figure 27 : Arrhenius plots for the γ-relaxation in the polyimide composite samples. Lines represent the best fits to the data

E_a values are within the typical reported range for the γ-relaxation in the polyimide which ranges approximately from 40–60 kJ/mol [152]. The activation energy value for the γ-relaxation drops significantly with the addition of only 0.5% clay, then exhibits a slight decrease for samples with increasing clay loading. It seems that clay facilitates the phenyl group oscilliations possibly by disturbing the rigid backbone chain packing.

Table 6 : Calculated activation energies for the γ-relaxation in the polyimide composite samples

Sample	Activation energy (kJ/mol)	Fit R^2
Pure PI	71.89	0.99
PI 0.5 clay	52.99	0.99
PI 2%clay	48.67	0.98
PI 3%clay	42.98	0.98

Secondary and Tg Relaxations in Polysulfone/Polyimide/Clay Composites

As noted above, both PSF and PI showed to be attractive for gas separation applications due to their thermal-oxidative stability, high T_gs, resistance to chemicals, mechanical properties, and solubility in organic solvent. However, there exist some issues related their usage for such application especially for PI which suffers from CO_2 plasticization in addition of being an expensive material. During operation above 8 bars, CO_2 swells the PI matrix and reduces the entangled chains effect leading to increased free volume and a reduction in membrane perm-selectivity. On the other hand, PSF demonstrated to resist plasticization above 30 bars of operating pressure and known to be of low cost [123].Thus, blending of PSF and PI is viable for gas separation membranes if one can find the right way to decrease their phase separation when blended. One way to do

so is to add a compatbilizer such as clay. The following section is a trial to understand the role of nanoclay in improving the dispersion of PSF/PI matrices within each other in the blend.

The powerful broadband dielectric spectroscopy technique is used to investigate the effect of nanoclay insertion on the secondary and T_g-related segmental motion of each polymer. Understanding and design of such intra- and inter-segmental mobility for PI, for example, was thought by Kim et al to be crucial for its gas separation performance as they affect membrane packing efficiency [52].

Figure 29 describes the temperature dependence of ε'' for the control PI and PSF samples as well as their blends with variable composition. Multiple relaxation processes are evident, to be exact, the secondary β relaxation in the PSF and PI, and the Tg-related motion in the PSF backbone. Assignment of these processes was detailed in the above sections for the PI/clay and PSF/clay composites.

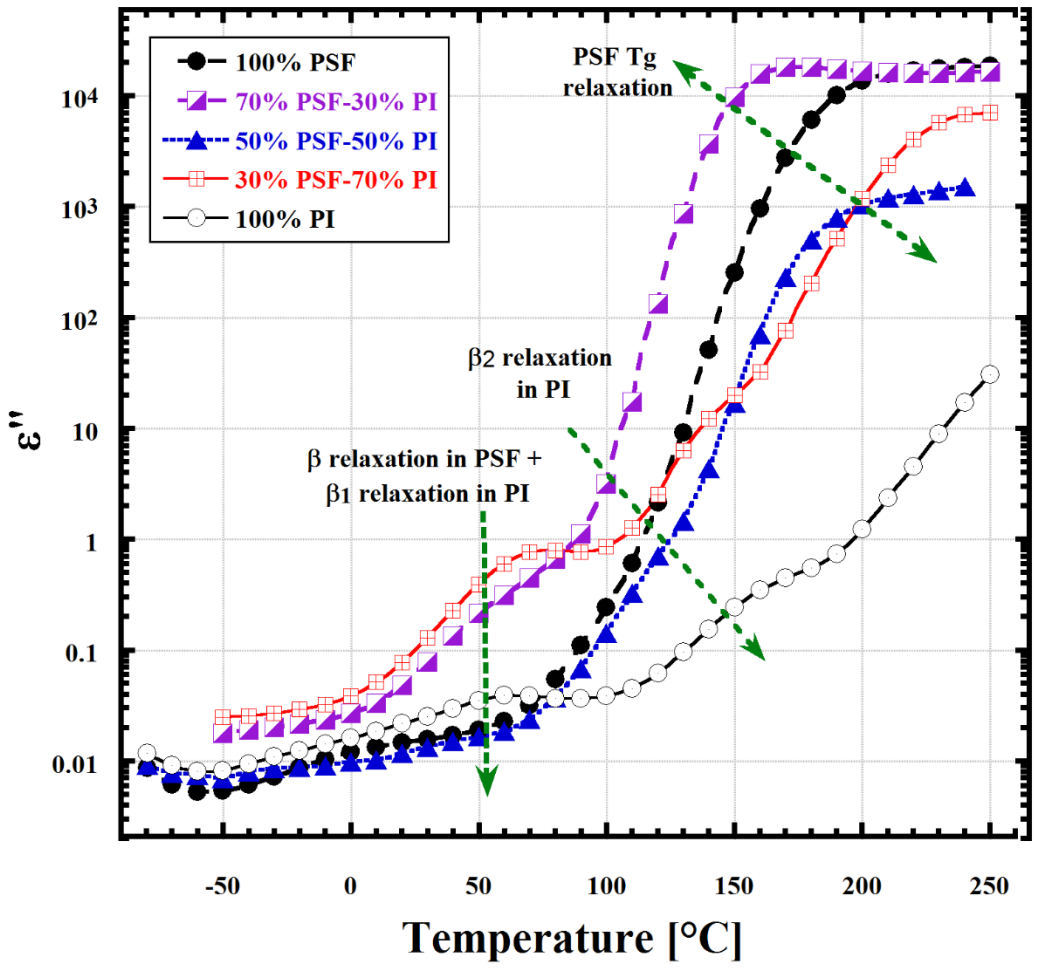

Figure 28: Temperature dependence of ε'' at 1 Hz for the PI, PSF, and their blends at different composition.

It is interesting to note that the β_2–relaxation of PI is only well resolved for the control PI and the blend containing 70% PI. While it appears to be very weak when the PI content is leass than 70%. This relaxation is linked to motions in the dianhydride segment of the chain [155] [156]. The weaking of this relaxation reveals that the dianhydride segment dipoles

find some movement constraints with increased PSF content. Ammar et al reported that the dispersed domain size of PSF/PI phases remarkably decrease with decreasing the PSF content in the blend [14]. A detailed investigation is currently in progress to clearly understand the PI's β_2–relaxation behavior in the blends. Around 50o C, there exist the PI's β_1–relaxation and the PSF's β–relaxation with their assigmnet as mentioned above.

The long-range segmental motion related to the PSF' Tg is clearly seen around 150 ^oC. This relaxation exhibit many interesting features. The observed difference in its intensity is related to samples thickness's variations, especially for the 50% PSF-50% PI sample which has the highest thickness. Thickness is reported to affect the dielectric response in ultrthin PSF films [135]. The second feature is that the peak maximum decreased as we moved from the control PSF to the 70% PSF-30% PI then increased with increasing the PI% in the blend. Rafiq et al. reported that the PSF' T_g increases as the content of PI is increased in the blend reflecting an improved stability [123]. Pure PI has a T_g of 302 ^oC [123] and its addition caused the blend Tg to increase as revealed by Figure 29. Also, the presence of a single Tg peak for the blend at different composition reflects the miscibility of the polymers at the molecular level [123, 157]. Finally, the initial decrease of the blend Tg after adding 30% PI could be explained in terms of the fact that PI would act as a plasticizer at this percent and certain amount of PI is required to triger the increase in the T_g. Further investigation is currently in progress to clarify this trend.

With addition of clay, for example to the 70% PSF-50% PI blend shown in Figure 30, the β–relaxations in PSF and PI does not seem to be altered for this composition. Also,

the Tg-related relaxation seems to exhibit the same position with no shifts except for the decrease in its intensity at 1% clay.

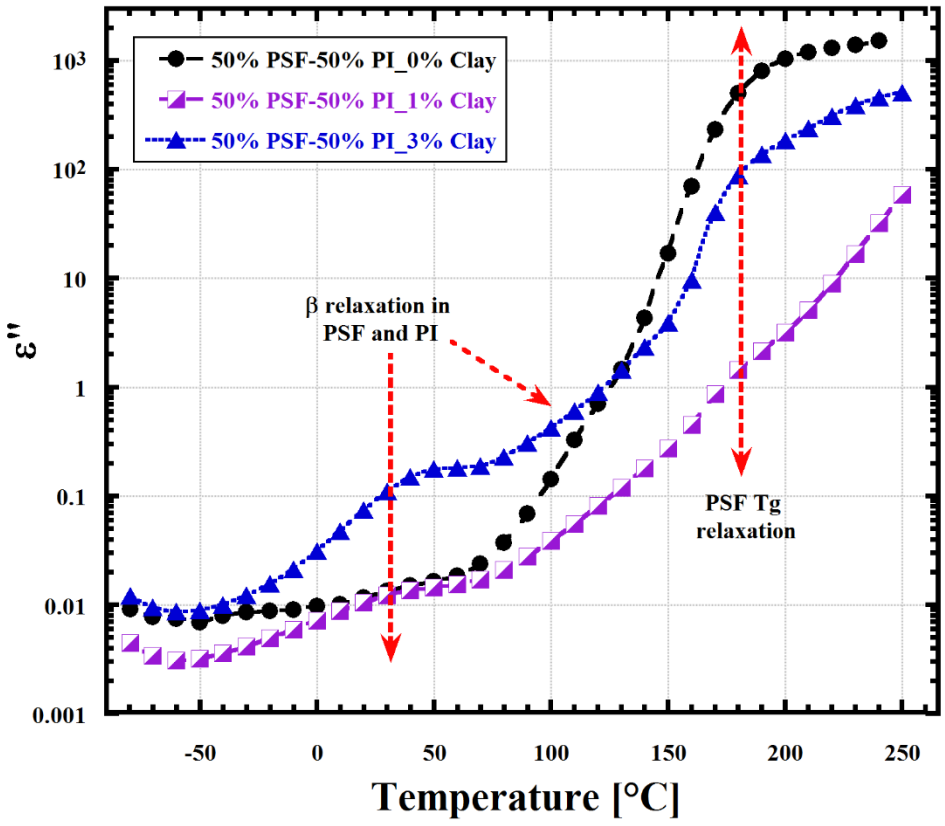

Figure 29: Temperature dependence of ε'' at 1 Hz for the 70% PSF-50% PI blend at different clay percents.

Figure 30 shows all the relaxation processes exhibited by the 70% PSF-50% PI-1% Clay sample as an example. Crests of the 3D ε''- f - T response surfaces, over a wide

temperature range of -80 to 250 °C are shown. The γ, β, and Tg-relaxation discussed above are clearly observable in Figure 30. Interestingly, an additional peak at low f is clear above the PSF' Tg which is thought be related to the MWS interfacial polarization effect. Since clay acts as a plsticizer for the blend, there will be some interfaces between the two polymers and between the organic polymeric matrix and the inorganic silicate layers of the clay. These different entities would cause differences in dielectric permittivity and/or charge conductivity across phase boundaries which results in fluctuating the interfacial polarization and an apparent peak related to this process appears at low f on loss permittivity ε'' vs. f plots.

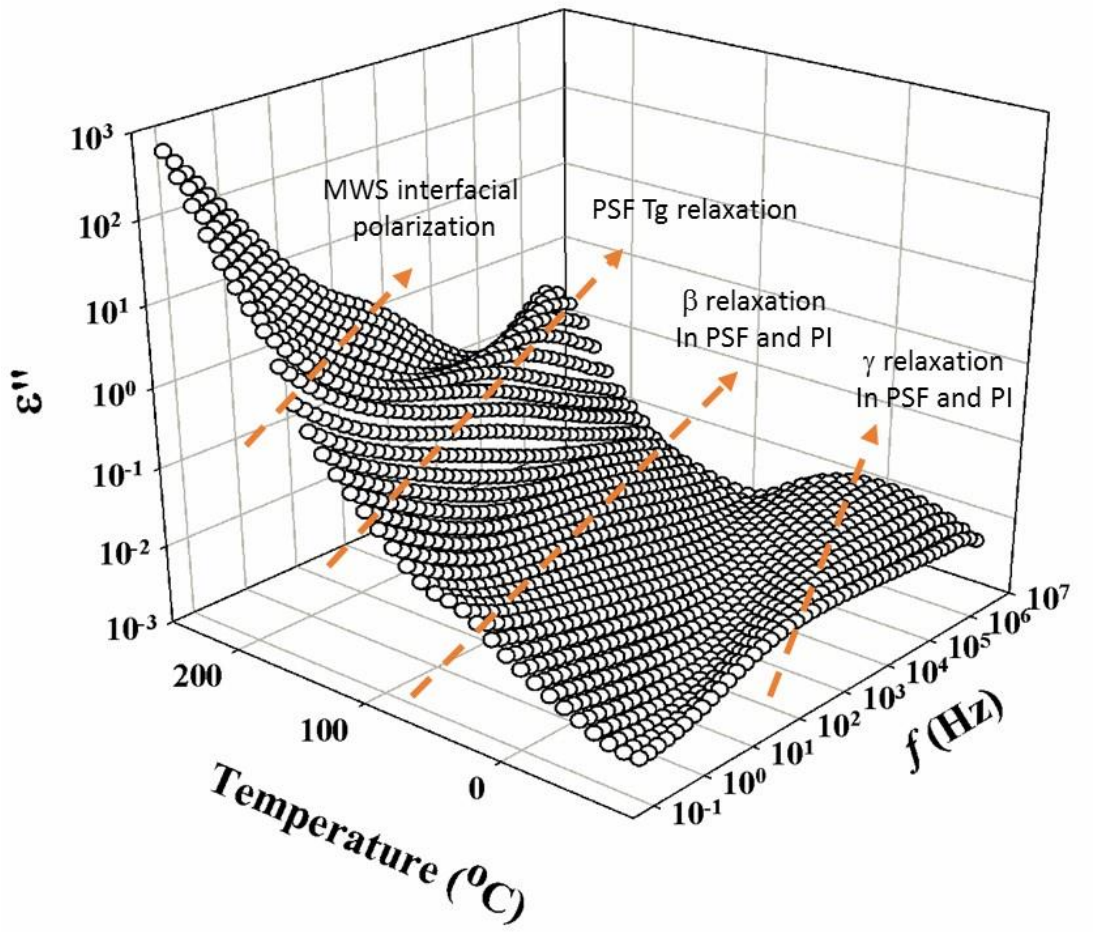

Figure 30: ε'' - f - T response surfaces for the 70% PSF-50% PI-1% Clay blend sample. Curves are spaced at 10° C increments and arrow follow the crests of different relaxations to show their progression with temperature

6. GAS BARRIER

Figure 31 shows oxygen flux, $J(t)$, curves obtained as a function of time for a) PSF/Cloisite 30B and b) PI/Cloisite 30B with different clay loadings at room temperature. The experimental data (open circles) and the fits (solid lines) showed the experimental data of oxygen flux were placed in the Fick's second law equation as fitting.

$$J(t) = \frac{P\Delta p}{l}\left[-\sum_{n=1}^{\infty}(-1)^n \exp\left(-\frac{D\pi^2 n^2 t}{l^2}\right)\right] \qquad \text{Equation [10]}$$

where Δp is the oxygen partial pressure difference, which was 1 atm in this case, l is the thickness of the membrane and t is the time. Previous studies have calculated the permeability P and diffusivity D using this equation [124], but in this study the permeability coefficient P was calculated directly from the steady-state flux J_∞ value (Equation 5).

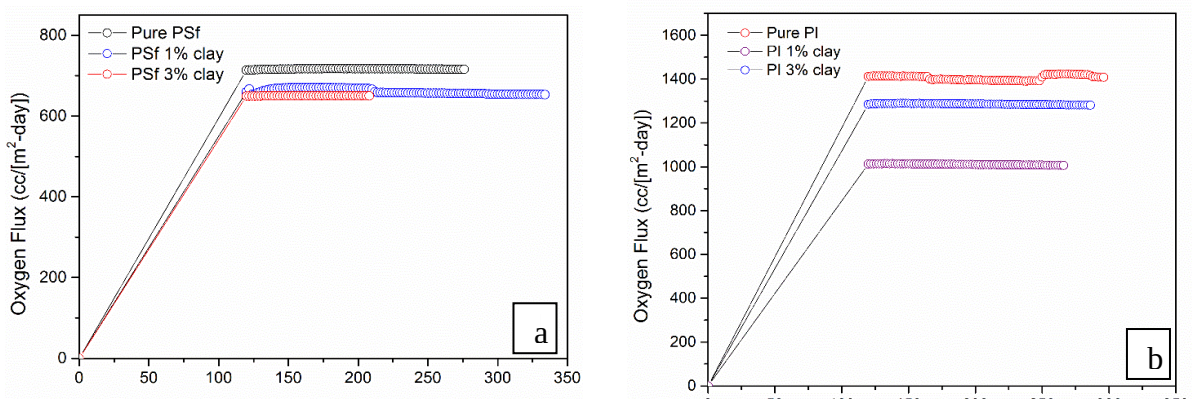

Figure 31: Oxygen permeability as a function of time for a) PSF composites, b) PI composites

The oxygen permeability values of the polysulfone/Cloisite 30B and polyimide/Cloisite 30B nanocomposites containing 1 and 3 wt% (nominal clay), are reported in Figure 32.

The results show that PSF with 1% clay has permeability = 1.5375 (cm^3/ [m^2-day]) while PI with 1% clay has permeability = 3.732 (cm^3/ [m^2-day]), indicating PSF has more than two-fold lower permeability than PI.

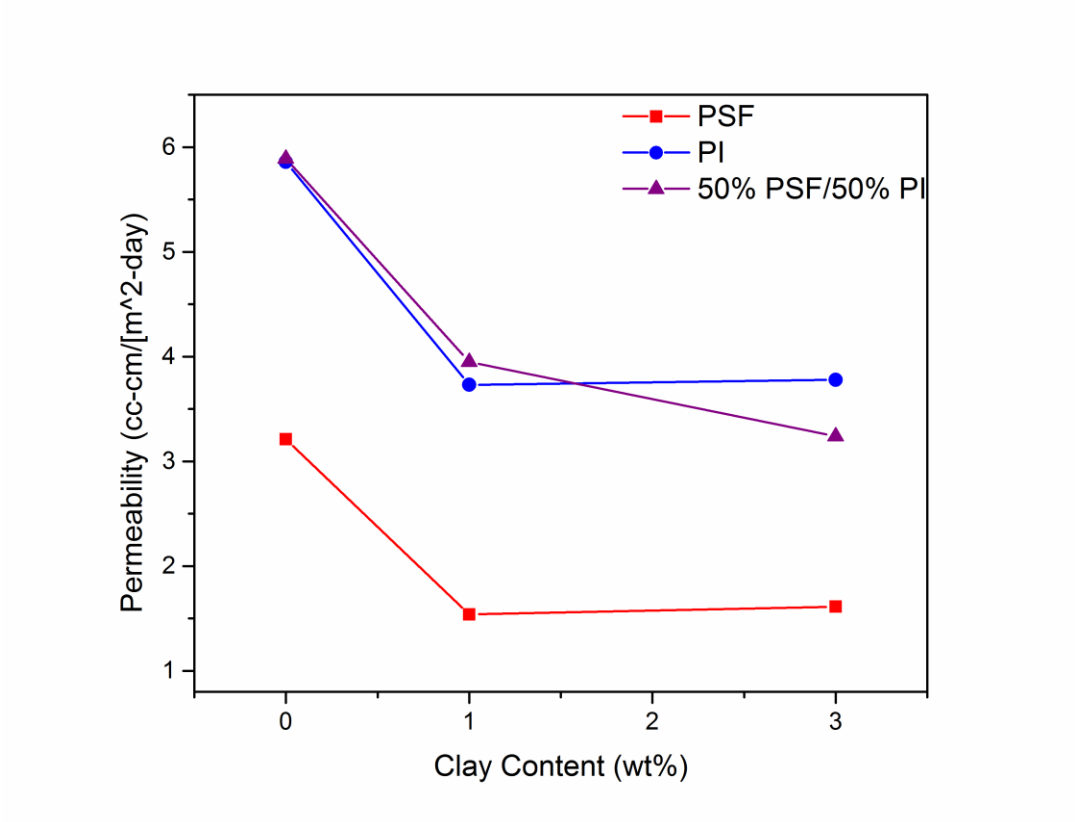

Figure 32: Oxygen permeability of polysulfone/Cloisite 30B and polyimide/Cloisite 30B as a function of clay loading

It should be noted that the permeability of PI membranes decreased by incorporating 1% of Cloisite® 30B and with even higher loadings, the permeability increased. When the clay content exceeds 3 wt.%, it is possible that there will be no significant effect of the clay content on permeation due to the aggregation phenomenon at high clay concentrations. It is worth mentioning that as the clay loading increases, the tortuosity factor will decrease and consequently lead to increasing the permeation [158, 159]. Previous studies explained the decreasing of oxygen permeability with decreasing the free volume and mobility and that decreasing could explained in terms of restricting the molecular level motions of biphenyl group in PI [54, 160, 161]. Here came the importance of dielectric spectroscopy to understand the movement of biphenyl group and its effect on the permeability.

There exist some other possibility for decreasing the permeability of oxygen with clay addition, some studies refers that the decreasing in oxygen permeability is due to some chemical interaction between the oxygen molecules and clay [162, 163]. And that is an acceptable explanation since oxygen molecules have partially negative charge and clay have partially positive charge and that will lead to attract the oxygen molecules and slower its diffusivity.

Figure 32 also show that blend of both polymer with 1:1 ratio. With 0% clay the blend in previous studies show immiscible morphology [14], and that might explain why the blend results is so close to polyimide results but still it need further more investigation to explain it. The permeability of oxygen is decreased very clearly when adding the clay and that can be explained from morphology point that adding the clay successfully overcome the phase

separation problem between the two polymers as the clay play as compatibilizer[101]. The homogenous blend of polymer with clay decrease the volume between the chains of polymers and hence decrease the permeability.

CHAPTER 5

5. CONCLUSION

In this work, PSF and PI with varied loadings of silicate nanocomposites has been presented for gas separation applications. More specifically, polymer nanocomposite films of PSF/Cloisite® 30B and PI/Cloisite® 30B were prepared via a doctor blade casting technique as a function of clay loading. The exfoliation of PSF and PI with Cloisite® 30B was evidenced from XRD which showed the loss of the characteristic clay diffraction peak.

Regarding gas separation, both composites showed a relatively high decrease in oxygen permeability when 1wt% of clay was added to the polymer matrix. On the other hand, samples with 3wt% clay composites did not give any significant results. It was also noted that PI composites have higher oxygen permeability than PSF due to the higher free volume between the PI chain with clay.

Broadband dielectric spectroscopy was used to probe macromolecular motions in polysulfone and its clay nanocomposites. The dynamics of chain motions related to the secondary γ-relaxation and the Tg long-range segmental mobility were analyzed in terms of the Havriliak-Negami model. The γ-relaxation is assigned to the local dipole swinging of the $–SO_2$ and the $–(CH_3)_2$ groups of the sulfone and the bisphenol sections of the polymer. Relaxation times were extracted from fitting the spectra to the H-N equation and then plotted against 1/T for all motions. The γ-relaxation exhibited an Arrhenius behavior while the Tg-related relaxation showed a non-Arrhenius VFTH trend. Vogel temperatures

extracted from the VFTH fitting of the spectra suggest a lower specific volume for the 0.5 and 2% clay samples. This outcome leads to the conclusion that more efficient chain packing is evident for these samples relative to the control PSF, thereby explaining the lower oxygen permeability results.

6. FUTURE WORK

The use of polyimide/polysulfone blends have been thoroughly studied for gas separation membrane applications [14, 93, 164–166]. Additionally, reported literature have discussed the incorporation of a filler such as zeolite [86] and silica [93] into a mixed matrix membrane of polyimide/polysulfone to ultimately increase system performance. . As such, a multi-component blend consisting of polyimide/polysulfone and Cloisite 30B is an interesting area to be further studied as potentially advanced nanocomposite membranes, especially from a gas separation point of view. Further research to study the selectivity of the films for different gas mixtures. In addition preparing a hollow fibers from the same material polyimide/clay and polysulfone/clay, since hollow fibers show a great and interesting result in field of gas separation [77, 88, 104, 147].

REFERENCES

[1] U.S. Energy Information Administration, "Qatar: International energy data and analysis," vol. 2015, pp. 1–16, 2015.

[2] leena kontaji T. Bob, "Worldwide Look at Reserves and Production," *Oil Gas J.*, vol. 113, no. 1b, p. 11, 2015.

[3] J. K. Adewole, A. L. Ahmad, S. Ismail, and C. P. Leo, "Current challenges in membrane separation of CO2 from natural gas: A review," *Int. J. Greenh. Gas Control*, vol. 17, pp. 46–65, 2013.

[4] P. Bernardo and E. Drioli, "Membrane gas separation progresses for process intensification strategy in the petrochemical industry," *Pet. Chem.*, vol. 50, no. 4, pp. 271–282, 2010.

[5] P. Bernardo, E. Drioli, and G. Golemme, "Membrane gas separation: A review/state of the art," *Ind. Eng. Chem. Res.*, vol. 48, no. 10, pp. 4638–4663, 2009.

[6] Jenkins, W. A., and K. R. Osborn, *Plastic Films: echnology and Packaging Applications*. CRC Press, 1992.

[7] J. Lange and Y. Wyser, "Recent innovations in barrier technologies for plastic packaging," *Packag. Technol. Sci.*, vol. 16, no. 4, pp. 149–158, 2003.

[8] M. A. Osman, V. Mittal, M. Morbidelli, and U. W. Suter, "Polyurethane Adhesive

Nanocomposites as Gas Permeation Barrier," *Macromolecules*, vol. 36, no. 26, pp. 9851–9858, Dec. 2003.

[9] S. Amberg-Schwab, M. Hoffmann, H. Bader, and M. Gessler, "Inorganic-Organic Polymers with Barrier Properties for Water Vapor, Oxygen and Flavors," *J. Sol-Gel Sci. Technol.*, vol. 13, no. 1, pp. 141–146.

[10] † Kostas S. Triantafyllidis, Peter C. LeBaron, In Park, and and Thomas J. Pinnavaia*, "Epoxy−Clay Fabric Film Composites with Unprecedented Oxygen-Barrier Properties," *Chem. Mater.*, vol. 18, no. 18, pp. 4393–4398, 2006.

[11] S. Anilkumar, M. G. Kumaran, and and Sabu Thomas, "Characterization of EVA/Clay Nanocomposite Membranes and Its Pervaporation Performance," *J. Phys. Chem. B*, vol. 112, no. 13, pp. 4009–4015, 2008.

[12] J.-M. Thomassin, C. Pagnoulle, G. Caldarella, A. Germain, and R. Jérôme, "Contribution of nanoclays to the barrier properties of a model proton exchange membrane for fuel cell application," *J. Memb. Sci.*, vol. 270, no. 1–2, pp. 50–56, Feb. 2006.

[13] B. Brulé and J.-J. Flat, "High Barrier Polyamide/Polyolefin/Organoclay Nanocomposites," *Macromol. Symp.*, vol. 233, no. 1, pp. 210–216, 2006.

[14] A. M. Ammar, "The Morphology and Mechanical Properties of Polysulfone/Polyimide Nanocomposite Films," 2012.

[15] M. Füllbrandt, S. Wellert, R. von Klitzing, and A. Schönhals, “Thermal and corrosion (in)stability of polyamide 6 studied by broadband dielectric spectroscopy,” *Polymer (Guildf).*, vol. 75, pp. 34–43, 2015.

[16] S. C. Tjong, “Structural and mechanical properties of polymer nanocomposites,” *Mater. Sci. Eng. R Reports*, vol. 53, no. 3–4, pp. 73–197, 2006.

[17] N. Alaslai, B. Ghanem, F. Alghunaimi, E. Litwiller, and I. Pinnau, “Pure- and Mixed-Gas Permeation Properties of Highly Selective and Plasticization Resistant Hydroxyl-Diamine-Based 6FDA Polyimides for CO2/CH4 Separation,” *J. Memb. Sci.*, vol. 505, pp. 100–107, 2016.

[18] H. Eguchi, D. J. Kim, and W. J. Koros, “Chemically cross-linkable polyimide membranes for improved transport plasticization resistance for natural gas separation,” *Polym. (United Kingdom)*, vol. 58, pp. 121–129, 2015.

[19] K.-S. Chang, C.-C. Tung, K.-S. Wang, and K.-L. Tung, “Free volume analysis and gas transport mechanisms of aromatic polyimide membranes: a molecular simulation study.,” *J. Phys. Chem. B*, vol. 113, no. 29, pp. 9821–30, 2009.

[20] E. K. Zhukova, A. A. Kuznetsov, M. Y. Yablokova, and A. Y. Alentiev, “Gas separation properties of new thermoplastic polyimides with phenylamide groups in diamine moiety: Effect of polymer structure,” *Pet. Chem.*, vol. 54, no. 7, pp. 544–550, 2014.

[21] Y. Zhuang, J. G. Seong, Y. S. Do, W. H. Lee, M. J. Lee, M. D. Guiver, and Y. M. Lee, "High-Strength, Soluble Polyimide Membranes Incorporating Tröger's Base for Gas Separation," *J. Memb. Sci.*, vol. 504, pp. 55–65, 2016.

[22] E. Rangel Rangel, E. M. Maya, F. Sánchez, J. de Abajo, and J. G. de la Campa, "Gas separation properties of mixed-matrix membranes containing porous polyimides fillers," *J. Memb. Sci.*, vol. 447, pp. 403–412, 2013.

[23] B. P. Singh, D. Singh, R. B. Mathur, and T. L. Dhami, "Influence of surface modified MWCNTs on the mechanical, electrical and thermal properties of polyimide nanocomposites," *Nanoscale Res. Lett.*, vol. 3, no. 11, pp. 444–453, 2008.

[24] J. H. Chang, K. M. Park, D. Cho, H. S. Yang, and K. J. Ihn, "Preparation and characterization of polyimide nanocomposites with different organo-montmorillonites," *Polym. Eng. Sci.*, vol. 41, no. 9, pp. 1514–1520, 2001.

[25] M. A. Osman, V. Mittal, and H. R. Lusti, "The Aspect Ratio and Gas Permeation in Polymer-Layered Silicate Nanocomposites," *Macromol. Rapid Commun.*, vol. 25, no. 12, pp. 1145–1149, 2004.

[26] D. Feldman, P. Kiliaris, C. D. Papaspyrides, L. a. Goettler, K. Y. Lee, H. Thakkar, C. W. Chiu, T. K. Huang, Y. C. Wang, B. G. Alamani, J. J. Lin, S. Sinha Ray, M. Okamoto, E. Manias, J. Jancar, J. F. Douglas, F. W. Starr, S. K. Kumar, P. Cassagnau, a. J. Lesser, S. S. Sternstein, M. J. Buehler, A. J. Crosby, J. Lee, T. K. Das, S. Prusty, L. a. Goettler, K. Y. Lee, H. Thakkar, W. Gacitua, A. Ballerini, J.

Zhang, P. Dubois, S. Rosset, S. Koster, J. Stauffer, S. Mikhaïlov, M. Dadras, N. F. D. Rooij, H. Shea, I. Zaman, B. Manshoor, A. Khalid, S. Araby, S. Pavlidou, and C. D. Papaspyrides, "Layered Silicate Reinforced Polymer Nanocomposites: Development and Applications," *Prog. Polym. Sci.*, vol. 47, no. 2, pp. 291–317, 2007.

[27] E. P. Giannelis, R. Krishnamoorti, and E. Manias, "Polymer-Silicate Nanocomposites : Model Systems for Confined Polymers and Polymer Brushes," *Polymer (Guildf).*, vol. 138, pp. 107–147, 1999.

[28] S. Pavlidou and C. D. Papaspyrides, "A review on polymer-layered silicate nanocomposites," *Prog. Polym. Sci.*, vol. 33, no. 12, pp. 1119–1198, 2008.

[29] T. Lan, P. D. Kaviratna, and T. J. Pinnavaia, "On the Nature of Polyimide-Clay Hybrid Composites," *Chem. Mater.*, vol. 6, no. 5, pp. 573–575, 1994.

[30] K. Yano, A. Usuki, and A. Okada, "Synthesis and properties of polyimide-clay hybrid films," *J. Polym. Sci. Part A Polym. Chem.*, vol. 35, no. 11, pp. 2289–2294, 1997.

[31] C. M. Zimmerman, A. Singh, and W. J. Koros, "Tailoring mixed matrix composite membranes for gas separations," *J. Memb. Sci.*, vol. 137, no. 1–2, pp. 145–154, Dec. 1997.

[32] H. Wang, B. A. Holmberg, and Y. Yan, "Homogeneous polymer–zeolite

nanocomposite membranes by incorporating dispersible template-removed zeolite nanocrystals," *J. Mater. Chem.*, vol. 12, no. 12, pp. 3640–3643, Nov. 2002.

[33] S. Kim, L. Chen, J. K. Johnson, and E. Marand, "Polysulfone and functionalized carbon nanotube mixed matrix membranes for gas separation: Theory and experiment," *J. Memb. Sci.*, vol. 294, no. 1–2, pp. 147–158, May 2007.

[34] E. A. Mason, "From pig bladders and cracked jars to polysulfones: an historical perspective on membrane transport," *J. Memb. Sci.*, vol. 60, no. 2, pp. 125–145, 1991.

[35] et al. Baker, R. W., "Membrane separation systems.," 1991.

[36] C. A. Scholes, S. E. Kentish, and G. W. Stevens, "Carbon Dioxide Separation through Polymeric Membrane Systems for Flue Gas Applications," *Recent Pat. Chem. Eng.*, vol. 1, no. 1, pp. 52–66, 2008.

[37] J. N. Barsema, S. D. Klijnstra, J. H. Balster, N. F. A. Van Der Vegt, G. H. Koops, and M. Wessling, "Intermediate polymer to carbon gas separation membranes based on Matrimid PI," *J. Memb. Sci.*, vol. 238, no. 1–2, pp. 93–102, 2004.

[38] T. M. G??r, "Permselectivity of zeolite filled polysulfone gas separation membranes," *J. Memb. Sci.*, vol. 93, no. 3, pp. 283–289, 1994.

[39] G. Maier, "Gas Separation with Polymer Membranes," *Angew. Chemie Int. Ed.*, vol. 37, no. 21, pp. 2960–2974, 1998.

[40] S. Sridhar, S. Bee, and S. K. Bhargava, “Membrane-based Gas Separation: Principle, Applications and Future Potential,” *Chem. Eng. Dig.*, pp. 1–25, 2014.

[41] W. J. Koros, “Barrier polymers and structures,” *Am. Chem. Soc.*, vol. 423, 1990.

[42] J. D. Perry, K. Nagai, and W. J. Koros, “Polymer Membranes for Hydrogen Separations,” *MRS Bull.*, vol. 31, no. 10, pp. 745–749, 2006.

[43] G. k. F. Koros, W. J., “membrane-based gas separation,” *J. Memb. Sci.*, vol. 83, no. 1, pp. 1–80, 1993.

[44] kamalesh k. sirkar, *Separation of Molecules, Macromolecules and Particles*. New York: Wiley-Interscience, 1975.

[45] J. C. Hill T., “Surface diffusion and thermal transpiration in fine tubes and pores,” no. 25, pp. 730–745, 1956.

[46] R. J. R. Uhlhorn, K. Keizer, and A. J. Burggraaf, “Gas transport and separation with ceramic membranes. Part I. Multilayer diffusion and capillary condensation,” *J. Memb. Sci.*, vol. 66, no. 2–3, pp. 259–269, 1992.

[47] W. J. Koros and G. K. Fleming, “Membrane-based gas separation,” *J. Memb. Sci.*, vol. 83, no. 1, pp. 1–80, 1993.

[48] B. FREEMAN and I. PINNAU, “Separation of gases using solubility-selective polymers,” *Trends Polym. Sci.*, vol. 5, no. 5, pp. 167–173, 1997.

[49] Yuri, Yampolskii, and B. Freeman, *Membrane Gas Separation*, Eds. Chichester, uk: John Wiley & Sons, Ltd, 2010.

[50] S. Alexander Stern, "Polymers for gas separations: the next decade," *J. Memb. Sci.*, vol. 94, no. 1, pp. 1–65, 1994.

[51] W. J. Koros, D. R. Paul, and A. A. Rocha, "Carbon dioxide sorption and transport in polycarbonate," *J. Polym. Sci. Polym. Phys. Ed.*, vol. 14, no. 4, pp. 687–702, Apr. 1976.

[52] T. H. Kim, W. J. Koros, G. R. Husk, and K. C. O'Brien, "Relationship between gas separation properties and chemical structure in a series of aromatic polyimides," *J. Memb. Sci.*, vol. 37, no. 1, pp. 45–62, 1988.

[53] K. Tanaka, H. Kita, M. Okano, and K. ichi Okamoto, "Permeability and permselectivity of gases in fluorinated and non-fluorinated polyimides," *Polymer (Guildf).*, vol. 33, no. 3, pp. 585–592, 1992.

[54] L. M. Robeson, "Correlation of separation factor versus permeability for polymeric membranes," *J. Memb. Sci.*, vol. 62, no. 2, pp. 165–185, 1991.

[55] M. R. Coleman and W. J. Koros, "Isomeric polyimides based on fluorinated dianhydrides and diamines for gas separation applications," *J. Memb. Sci.*, vol. 50, no. 3, pp. 285–297, 1990.

[56] M. Salame, "Prediction of gas barrier properties of high polymers," *Polym. Eng.*

Sci., vol. 26, no. 22, pp. 1543–1546, 1986.

[57] J. Bicerano, “Macromolecules containing metal and ?metal-like? elements, Volume 2, Organoiron Polymers. Edited by Alaa S Abd-El-Aziz, Charles E Carraher, Jr, Charles U Pittman, Jr, John E Sheats and Martel Zeldin. John Wiley & Sons, New York, 2003. ISBN 0-471-45078,” *Polym. Int.*, vol. 54, no. 1, pp. 246–246, 2005.

[58] W. M. Lee, “Selection of barrier materials from molecular structure,” *Polym. Eng. Sci.*, vol. 20, no. 1, pp. 65–69, 1980.

[59] M. W. Hellums, W. J. Koros, G. R. Husk, and D. R. Paul, “Fluorinated polycarbonates for gas separation applications,” *J. Memb. Sci.*, vol. 46, no. 1, pp. 93–112, 1989.

[60] M. R. Pixton and D. R. Paul, “Gas Transport Properties of Polyarylates: Substituent Size and Symmetry Effects,” *Macromolecules*, vol. 28, no. 24, pp. 8277–8286, 1995.

[61] P. Bernardo and G. Clarizia, “30 Years of Membrane Technology for Gas Separation,” *Icheap-11 11th Int. Conf. Chem. Process Eng. Pts 1-4*, vol. 32, pp. 1999–2004, 2013.

[62] R. Nasir, H. Mukhtar, Z. Man, and D. F. Mohshim, “Material Advancements in Fabrication of Mixed-Matrix Membranes,” *Chem. Eng. Technol.*, vol. 36, no. 5, pp.

717–727, 2013.

[63] H. A. Mannan, H. Mukhtar, T. Murugesan, R. Nasir, D. F. Mohshim, and A. Mushtaq, “Recent Applications of Polymer Blends in Gas Separation Membranes,” *Chem. Eng. Technol.*, vol. 36, no. 11, pp. 1838–1846, 2013.

[64] a. Mushtaq, H. Mukhtar, a. M. Shariff, and H. a. Mannan, “A Review : Development of Polymeric Blend Membrane for Removal of CO 2 from Natural Gas,” *Int. J. Eng. Technol. IJET-IJENS*, vol. 13, no. 02, pp. 53–60, 2013.

[65] Y. P. Y. Donald R. Paul, *Polymeric Gas Separation Membranes*. london: CRC Press, 1993.

[66] “Technology of Polymers,” pp. 821–834, 1998.

[67] H. Borjigin, Q. Liu, W. Zhang, K. Gaines, J. S. Riffle, D. R. Paul, B. D. Freeman, and J. E. McGrath, “Synthesis and characterization of thermally rearranged (TR) polybenzoxazoles: Influence of isomeric structure on gas transport properties,” *Polym. (United Kingdom)*, vol. 75, pp. 199–210, 2015.

[68] T. Sakaguchi, Y. Shinoda, and T. Hashimoto, “Synthesis and gas permeability of nitrated and aminated Poly(diphenylacetylene)s,” *Polym. (United Kingdom)*, vol. 55, no. 26, pp. 6680–6685, 2014.

[69] A. L. Khan, A. Cano-Odena, B. Guti??rrez, C. Minguill??n, and I. F. J. Vankelecom, “Hydrogen separation and purification using polysulfone acrylate-zeolite mixed

matrix membranes," *J. Memb. Sci.*, vol. 350, no. 1–2, pp. 340–346, 2010.

[70] M. Minelli and G. C. Sarti, "Gas permeability in glassy polymers: A thermodynamic approach," *Fluid Phase Equilib.*, pp. 1–8, 2015.

[71] S. Basu, A. Cano-Odena, and I. F. J. Vankelecom, "MOF-containing mixed-matrix membranes for CO2/CH4 and CO2/N2 binary gas mixture separations," *Sep. Purif. Technol.*, vol. 81, no. 1, pp. 31–40, 2011.

[72] E. M. Erdni-Goryaev, a. Y. Alent'ev, a. S. Shaplov, D. O. Ponkratov, and E. I. Lozinskaya, "New membrane materials based on crosslinked poly(ethylene glycols) and ionic liquids for separation of gas mixtures containing CO2," *Polym. Sci. Ser. B*, vol. 56, no. 6, pp. 900–908, 2014.

[73] K. N. Shinji Kanehashi, Shuichi Sato, "synthesis and Gas Permeability of Hyperbranched and Cross-Linked Polyimide Membranes," UK: John Wiley & Sons, Ltd, 2010.

[74] T. Nakagawa, T. Nishimura, and A. Higuchi, "Morphology and gas permeability in copolyimides containing polydimethylsiloxane block," *J. Memb. Sci.*, vol. 206, no. 1–2, pp. 149–163, 2002.

[75] P. B. Containing, *Polymer Blends Handbook, Volume 2*. 2014.

[76] H. B. Park, S. H. Han, C. H. Jung, Y. M. Lee, and A. J. Hill, "Thermally rearranged (TR) polymer membranes for CO2 separation," *J. Memb. Sci.*, vol. 359, no. 1–2, pp.

11–24, 2010.

[77] S. S. Hosseini, N. Peng, and T. S. Chung, “Gas separation membranes developed through integration of polymer blending and dual-layer hollow fiber spinning process for hydrogen and natural gas enrichments,” *J. Memb. Sci.*, vol. 349, no. 1–2, pp. 156–166, 2010.

[78] D. Q. Vu, W. J. Koros, and S. J. Miller, “Mixed matrix membranes using carbon molecular sieves,” *J. Memb. Sci.*, vol. 211, no. 2, pp. 311–334, 2003.

[79] A. Dehghani Kiadehi, A. Rahimpour, M. Jahanshahi, and A. A. Ghoreyshi, “Novel carbon nano-fibers (CNF)/polysulfone (PSf) mixed matrix membranes for gas separation,” *J. Ind. Eng. Chem.*, vol. 22, pp. 199–207, 2015.

[80] M. KARĞILI, “POLYMER BLEND BASED MIXED MATRIX GAS SEPARATION MEMBRANES,” MIDDLE EAST TECHNICAL UNIVERSITY, 2015.

[81] G. Clarizia, C. Algieri, and E. Drioli, “Filler-polymer combination: A route to modify gas transport properties of a polymeric membrane,” *Polymer (Guildf).*, vol. 45, no. 16, pp. 5671–5681, 2004.

[82] H. Abdul Mannan, H. Mukhtar, M. Shima Shaharun, M. Roslee Othman, and T. Murugesan, “Polysulfone/poly(ether sulfone) blended membranes for CO2 separation,” *J. Appl. Polym. Sci.*, vol. 133, no. 5, pp. 1–9, 2016.

[83] N. A. Ahmad, C. P. Leo, A. L. Ahmad, and A. W. Mohammad, “Separation of CO2 from hydrogen using membrane gas absorption with PVDF/PBI membrane,” *Int. J. Hydrogen Energy*, vol. 41, no. 8, pp. 4855–4861, 2015.

[84] H. Rabiee, A. Ghadimi, S. Abbasi, and T. Mohammadi, “CO2 separation performance of poly(ether-b-amide6)/PTMEG blended membranes: Permeation and sorption properties,” *Chem. Eng. Res. Des.*, vol. 98, pp. 96–106, 2015.

[85] V. Giel, J. Kredatusová, M. Trchová, J. Brus, J. Žitka, and J. Peter, “Polyaniline/polybenzimidazole blends: Characterisation of its physico-chemical properties and gas separation behaviour,” *Eur. Polym. J.*, 2016.

[86] F. Dorosti, M. R. Omidkhah, M. Z. Pedram, and F. Moghadam, “Fabrication and characterization of polysulfone/polyimide-zeolite mixed matrix membrane for gas separation,” *Chem. Eng. J.*, vol. 171, no. 3, pp. 1469–1476, 2011.

[87] H. Karkhanechi, H. Kazemian, H. Nazockdast, M. R. Mozdianfard, and S. M. Bidoki, “Fabrication of Homogenous Polymer-Zeolite Nanocomposites as Mixed-Matrix Membranes for Gas Separation,” *Chem. Eng. Technol.*, vol. 35, no. 5, pp. 885–892, 2012.

[88] M. VM, A. LG, F. A, and S. SJ, “Polysulfone mixed matrix gas separation hollow fibre membranes filled with polymer and carbon xerogels,” *Chem. Eng. Sci.*, vol. 92, pp. 13–20, 2013.

[89] L. Liang, Q. Gan, and P. Nancarrow, “Composite ionic liquid and polymer membranes for gas separation at elevated temperatures,” *J. Memb. Sci.*, vol. 450, pp. 407–417, 2014.

[90] F. Xiang, P. Tzeng, J. S. Sawyer, O. Regev, and J. C. Grunlan, “Improving the gas barrier property of clay-polymer multilayer thin films using shorter deposition times,” *ACS Appl. Mater. Interfaces*, vol. 6, no. 9, pp. 6040–6048, 2014.

[91] A. R. Moghadassi, Z. Rajabi, S. M. Hosseini, and M. Mohammadi, “Preparation and Characterization of (PVC-Blend-SBR) Mixed Matrix Gas Separation Membrane Filled with Zeolite,” *Arab. J. Sci. Eng.*, vol. 39, no. 2, pp. 605–614, 2014.

[92] M. Wang, Z. Wang, N. Li, J. Liao, S. Zhao, J. Wang, and S. Wang, “Relationship between polymer-filler interfaces in separation layers and gas transport properties of mixed matrix composite membranes,” *J. Memb. Sci.*, vol. 495, pp. 252–268, 2015.

[93] S. Rafiq, Z. Man, A. Maulud, N. Muhammad, and S. Maitra, “Separation of CO2 from CH4 using polysulfone/polyimide silica nanocomposite membranes,” *Sep. Purif. Technol.*, vol. 90, pp. 162–172, 2012.

[94] T. H. Bae, J. S. Lee, W. Qiu, W. J. Koros, C. W. Jones, and S. Nair, “A high-performance gas-separation membrane containing submicrometer-sized metal-organic framework crystals,” *Angew. Chemie - Int. Ed.*, vol. 49, no. 51, pp. 9863–9866, 2010.

[95] A. J. Crosby and J.-Y. Lee, “Polymer Nanocomposites: The ‘Nano’ Effect on Mechanical Properties.,” *Polym. Rev.*, vol. 47, no. 2, pp. 217–219, 2007.

[96] B. Chen, J. R. G. Evans, H. C. Greenwell, P. Boulet, P. V Coveney, A. A. Bowden, and A. Whiting, “A critical appraisal of polymer-clay nanocomposites.,” *Chem. Soc. Rev.*, vol. 37, no. 3, pp. 568–94, Mar. 2008.

[97] S. Sen, J. D. Thomin, S. K. Kumar, and P. Keblinski, “Molecular Underpinnings of the Mechanical Reinforcement in Polymer Nanocomposites,” *Macromolecules*, vol. 40, no. 11, pp. 4059–4067, May 2007.

[98] T. D. Fornes, P. J. Yoon, H. Keskkula, and D. R. Paul, “Nylon 6 nanocomposites: the effect of matrix molecular weight,” *Polymer (Guildf).*, vol. 42, no. 25, pp. 09929–09940, Dec. 2001.

[99] Y. Zare and H. Garmabi, “Thickness, modulus and strength of interphase in clay/polymer nanocomposites,” *Appl. Clay Sci.*, vol. 105–106, pp. 66–70, Mar. 2015.

[100] O. C. Wokadala, S. S. Ray, J. Bandyopadhyay, J. Wesley-Smith, and N. M. Emmambux, “Morphology, thermal properties and crystallization kinetics of ternary blends of the polylactide and starch biopolymers and nanoclay: The role of nanoclay hydrophobicity,” *Polymer (Guildf).*, vol. 71, pp. 82–92, Aug. 2015.

[101] H. M. Tiggemann, V. F. Ribeiro, F. Celso, and S. M. B. Nachtigall, “Effect of

commercial clays on the properties of SEBS/PP/oil thermoplastic elastomers. Part 1. Physical, mechanical and thermal properties," *Appl. Clay Sci.*, vol. 109–110, pp. 151–156, Jun. 2015.

[102] H. Assaedi, F. U. A. Shaikh, and I. M. Low, "Effect of nano-clay on mechanical and thermal properties of geopolymer," *J. Asian Ceram. Soc.*, vol. 4, no. 1, pp. 19–28, Mar. 2016.

[103] Y. Li, H. M. Guan, T. S. Chung, and S. Kulprathipanja, "Effects of novel silane modification of zeolite surface on polymer chain rigidification and partial pore blockage in polyethersulfone (PES)-zeolite A mixed matrix membranes," *J. Memb. Sci.*, vol. 275, no. 1–2, pp. 17–28, 2006.

[104] S. Husain, "Mixed Matrix Dual Layer Hollow Fiber Membranes for Natural Gas Separation," *Text. Eng.*, no. August, pp. 1–214, 2006.

[105] M. A. Priolo, D. Gamboa, K. M. Holder, and J. C. Grunlan, "Super gas barrier of transparent polymer-clay multilayer ultrathin films.," *Nano Lett.*, vol. 10, no. 12, pp. 4970–4, Dec. 2010.

[106] G. H. Fredrickson and J. Bicerano, "Barrier properties of oriented disk composites," *J. Chem. Phys.*, vol. 110, no. 4, p. 2181, 1999.

[107] A. Usuki, Y. Kojima, M. Kawasumi, A. Okada, Y. Fukushima, T. Kurauchi, and O. Kamigaito, "Synthesis of nylon 6-clay hybrid," *J. Mater. Res.*, vol. 8, no. 05, pp.

1179–1184, Jan. 2011.

[108] H. J. Ploehn and C. Liu, “Quantitative Analysis of Montmorillonite Platelet Size by Atomic Force Microscopy,” *Ind. Eng. Chem. Res.*, vol. 45, no. 21, pp. 7025–7034, Oct. 2006.

[109] L. E. Nielsen, “Models for the Permeability of Filled Polymer Systems,” *J. Macromol. Sci. Part A - Chem.*, vol. 1, no. 5, pp. 929–942, Aug. 1967.

[110] E. L. Cussler, S. E. Hughes, W. J. Ward, and R. Aris, “Barrier membranes,” *J. Memb. Sci.*, vol. 38, no. 2, pp. 161–174, Aug. 1988.

[111] A. Gurses, *Introduction to Polymer–Clay Nanocomposites*, 1st ed. Turky: CRC Press, 2015.

[112] M. A. Osman, V. Mittal, and U. W. Suter, “Poly(propylene)-Layered Silicate Nanocomposites: Gas Permeation Properties and Clay Exfoliation,” *Macromol. Chem. Phys.*, vol. 208, no. 1, pp. 68–75, Jan. 2007.

[113] J. KIM, C. HU, R. WOO, and M. SHAM, “Moisture barrier characteristics of organoclay?epoxy nanocomposites,” *Compos. Sci. Technol.*, vol. 65, no. 5, pp. 805–813, Apr. 2005.

[114] E. PICARD, A. VERMOGEN, J. GERARD, and E. ESPUCHE, “Barrier properties of nylon 6-montmorillonite nanocomposite membranes prepared by melt blending: Influence of the clay content and dispersion stateConsequences on modelling,” *J.*

Memb. Sci., vol. 292, no. 1–2, pp. 133–144, Apr. 2007.

[115] J. W. B. and D. R. P. T. D. Traugott, "Mechanical compatibilization of high density polyethylene–poly(ethylene terephthalate) blends," *J. Appl. Polym. Sci.*, vol. 28, no. 9, pp. 2947–2959, 1983.

[116] Hugh R. Brown, "Effect of a diblock copolymer on the adhesion between incompatible polymers," *Macromolecules*, vol. 22, no. 6, pp. 2859–2860, 1989.

[117] L. M. Robeson, "Polymer Blends: A Comprehensive Review," *Carl Hanser GmbH*, pp. 10–23, 2007.

[118] D.R. Paul, *Polymer blends containing styrene/hydrogenated butadiene block copolymers: solubilization and compatibilization*, 2nd ed. Munich: Hanser Publishers, 1996.

[119] C. B. B. D.R. Paul, "volume 2: Performance," in *polymer blends:Formulation and Performance*, 2nd ed., New York: Wiley, 2000.

[120] A. Ophir, L. Zonder, and P. F. Rios, "Thermodynamic characterization of hybrid polymer blend systems.," *Polym. Eng. Sci.*, vol. 49, no. 6, pp. 1168–1176, 2009.

[121] O. Monticelli, A. Bottino, I. Scandale, G. Capannelli, and Saverio Russo, "Preparation and Properties of Polysulfone–Clay Composite Membranes," *J. Appl. Polym. Sci.*, vol. 103, pp. 3637–3644, 2006.

[122] solvay, “Udel ® P-1700,” 2016. [Online]. Available: http://catalog.ides.com/Datasheet.aspx?E=25478&FMT=PDF&I=92041&U=0.

[123] S. Rafiq, Z. Man, A. Maulud, N. Muhammad, and S. Maitra, “Effect of varying solvents compositions on morphology and gas permeation properties on membranes blends for CO2 separation from natural gas,” *J. Memb. Sci.*, vol. 378, no. 1–2, pp. 444–452, 2011.

[124] D. J. Sekelik, E. V Stepanov, S. Nazarenko, D. Schiraldi, A. Hiltner, and E. Baer, “Oxygen barrier properties of crystallized and talc-filled poly(ethylene terephthalate),” *J. Polym. Sci. Part B Polym. Phys.*, vol. 37, no. 8, pp. 847–857, 1999.

[125] S. Havriliak and S. Negami, “A complex plane representation of dielectric and mechanical relaxation processes in some polymers,” *Polymer (Guildf).*, vol. 8, pp. 161–210, Jan. 1967.

[126] S. Havriliak and S. J. Havriliak, “Comparison of the Havriliak-Negami and stretched exponential functions,” *Polymer (Guildf).*, vol. 37, no. 18, pp. 4107–4110, 1996.

[127] M. T. Viciosa, M. Dionísio, R. M. Silva, R. L. Reis, and J. F. Mano, “Molecular motions in chitosan studied by dielectric relaxation spectroscopy.,” *Biomacromolecules*, vol. 5, no. 5, pp. 2073–8, 2004.

[128] K. a. Mauritz, “Dielectric Relaxation Studies of Ion Motions in Electrolyte-

Containing Perfluorosulfonate Ionomers. 4. Long-Range Ion Transport," *Macromolecules*, vol. 22, no. 37, pp. 4483–4488, 1989.

[129] F. Kremer and A. Schönhals, *Broadband Dielectric Spectroscopy*. Berlin, Heidelberg: Springer Berlin Heidelberg, 2003.

[130] T. N. Blanton, D. Majumdar, and S. M. Melpolder, "MICROSTRUCTURE OF CLAY-POLYMER COMPOSITES," *Appl. X-ray Anal.*, vol. 42, no. 1, pp. 562–568, 2009.

[131] S. J. Osborn, M. K. Hassan, G. M. Divoux, D. W. Rhoades, K. a. Mauritz, and R. B. Moore, "Glass transition temperature of perfluorosulfonic acid ionomers," *Macromolecules*, vol. 40, no. 10, pp. 3886–3890, 2007.

[132] J. S. Wiggins, M. K. Hassan, K. a. Mauritz, and R. F. Storey, "Hydrolytic degradation of poly(d,l-lactide) as a function of end group: Carboxylic acid vs. hydroxyl," *Polymer (Guildf).*, vol. 47, no. 6, pp. 1960–1969, 2006.

[133] I. D. Stefanithis and K. a. Mauritz, "Microstructural evolution of a silicon oxide phase in a perfluorosulfonic acid ionomer by an in situ sol-gel reaction. 3. Thermal analysis studies," *Macromolecules*, vol. 23, pp. 2397–2402, 1990.

[134] D. Radloff, C. Boeffel, and H. W. Spiess, "Cellulose and Cellulose/Poly(vinyl alcohol) Blends. 2. Water Organization Revealed by Solid-State NMR Spectroscopy," *Macromolecules*, vol. 29, no. 5, pp. 1528–1534, 1996.

[135] D. Labahn, R. Mix, and A. Schönhals, “Dielectric relaxation of ultrathin films of supported polysulfone,” *Phys. Rev. E - Stat. Nonlinear, Soft Matter Phys.*, vol. 79, no. 1, pp. 1–9, 2009.

[136] J. Tsuwi, D. Pospiech, D. Jehnichen, L. Häußler, and F. Kremer, “Molecular dynamics in semifluorinated-side-chain polysulfone studied by broadband dielectric spectroscopy,” *J. Appl. Polym. Sci.*, vol. 105, no. 1, pp. 201–207, Jul. 2007.

[137] A. F. Yee and S. A. Smith, “Molecular structure effects on the dynamic mechanical spectra of polycarbonates,” *Macromolecules*, vol. 14, no. 1, pp. 54–64, Jan. 1981.

[138] C. L. Aitken, J. S. McHattie, and D. R. Paul, “Dynamic mechanical behavior of polysulfones,” *Macromolecules*, vol. 25, no. 11, pp. 2910–2922, May 1992.

[139] K. Varadarajan and R. F. Boyer, “Effects of thermal history, crystallinity, and solvent on the transitions and relaxations in poly(bisphenol-A carbonate),” *J. Polym. Sci. Polym. Phys. Ed.*, vol. 20, no. 1, pp. 141–154, Jan. 1982.

[140] J. W. Kang, K. Choi, W. H. Jo, and S. L. Hsu, “Structure–property relationships of polyimides: a molecular simulation approach,” *Polymer (Guildf).*, vol. 39, no. 26, pp. 7079–7087, Dec. 1998.

[141] J. R. Fried, A. Letton, and W. J. Welsh, “Secondary relaxation processes in bisphenol-A polysulphone,” *Polymer (Guildf).*, vol. 31, no. 6, pp. 1032–1037, Jun. 1990.

[142] R. J. Klein, S. Zhang, S. Dou, B. H. Jones, R. H. Colby, and J. Runt, "Modeling electrode polarization in dielectric spectroscopy: Ion mobility and mobile ion concentration of single-ion polymer electrolytes.," *J. Chem. Phys.*, vol. 124, no. 14, p. 144903, Apr. 2006.

[143] H. Chen, M. K. Hassan, S. K. Peddini, and K. A. Mauritz, "Macromolecular dynamics of sulfonated poly(styrene-b-ethylene-ran-butylene-b-styrene) block copolymers by broadband dielectric spectroscopy," *Eur. Polym. J.*, vol. 47, no. 10, pp. 1936–1948, Oct. 2011.

[144] S. Zhang and J. Runt, "Segmental Dynamics and Ionic Conduction in Poly(vinyl methyl ether)−Lithium Perchlorate Complexes," Apr. 2004.

[145] H. Vogel, "The law of the relation between the viscosity of liquids and the temperature," *Phys. Zeitschrift*, vol. 22, pp. 645–646, 1921.

[146] Y. Huang and D. R. Paul, "Physical Aging of Thin Glassy Polymer Films Monitored by Optical Properties," *Macromolecules*, vol. 39, no. 4, pp. 1554–1559, Feb. 2006.

[147] W. C. Madden, D. Punsalan, and W. J. Koros, "Age dependent CO2 sorption in Matrimid® asymmetric hollow fiber membranes," *Polymer (Guildf).*, vol. 46, no. 15, pp. 5433–5436, Jul. 2005.

[148] A. D. Drozdov, "The effect of temperature on physical aging of glassy polymers," *J. Appl. Polym. Sci.*, vol. 81, no. 13, pp. 3309–3320, Sep. 2001.

[149] J. M. Hutchinson, “Physical aging of polymers,” *Prog. Polym. Sci.*, vol. 20, no. 4, pp. 703–760, Jan. 1995.

[150] J. P. Habas, J. Peyrelasse, and M. F. Grenier-Loustalot, “Rheological Study of a High-Performance Polyimide. Interpretation of the Secondary Mechanical Relaxations of a Nadimide Crosslinked System,” *High Perform. Polym.* , vol. 8 , no. 4 , pp. 515–532, Dec. 1996.

[151] S. Z. D. Cheng, T. M. Chalmers, Y. Gu, Y. Yoon, F. W. Harris, J. Cheng, M. Fone, and J. L. Koenig, “Relaxation processes and molecular motion in a new semicrystalline polyimide,” *Macromol. Chem. Phys.*, vol. 196, no. 5, pp. 1439–1451, May 1995.

[152] A. C. Comer, D. S. Kalika, B. W. Rowe, B. D. Freeman, and D. R. Paul, “Dynamic relaxation characteristics of Matrimid® polyimide,” *Polymer (Guildf).*, vol. 50, no. 3, pp. 891–897, Jan. 2009.

[153] F. E. Arnold, K. R. Jr.Bruno, D. Shen, M. Eashoo, C. J. Lee, F. W. Harris, and S. Z. . Cheng, “The Origin of b Relaxations in Segmented Rigid-Rod Polyimide and Copolyimide Films,” *Polym. Eng. Sci.*, vol. 33, p. 1373, 1993.

[154] Z. Sun, L. Dong, Y. Zhuang, L. Cao, M. Ding, and Z. Feng, “Beta relaxation in polyimides,” *Polymer (Guildf).*, vol. 33, no. 22, pp. 4728–4731, Jan. 1992.

[155] F. Li, J. J. Ge, P. S. Honigfort, S. Fang, J.-C. Chen, F. W. Harris, and S. Z. D. Cheng,

"Dianhydride architectural effects on the relaxation behaviors and thermal and optical properties of organo-soluble aromatic polyimide films," *Polymer (Guildf).*, vol. 40, no. 18, pp. 4987–5002, Aug. 1999.

[156] W.-L. Qu, T.-M. Ko, R. H. Vora, and T.-S. Chung, "Anisotropic dielectric properties of polyimides consisting of various molar ratios ofmeta topara diamine with trifluoromethyl group," *Polym. Eng. Sci.*, vol. 41, no. 10, pp. 1783–1793, Oct. 2001.

[157] A. Linares and J. L. Acosta, "Structural characterization of polymer blends based on polysulfones," *J. Appl. Polym. Sci.*, vol. 92, no. 5, pp. 3030–3039, Jun. 2004.

[158] K. E. Strawhecker and E. Manias, "Structure and Properties of Poly(vinyl alcohol)/Na + Montmorillonite Nanocomposites," *Chem. Mater.*, vol. 12, no. 10, pp. 2943–2949, Oct. 2000.

[159] R. K. Bharadwaj, "Modeling the Barrier Properties of Polymer-Layered Silicate Nanocomposites," *Macromolecules*, vol. 34, no. 26, pp. 9189–9192, Dec. 2001.

[160] Y. Hirayama, T. Yoshinaga, Y. Kusuki, K. Ninomiya, T. Sakakibara, and T. Tamari, "Relation of gas permeability with structure of aromatic polyimides I," *J. Memb. Sci.*, vol. 111, no. 2, pp. 169–182, Mar. 1996.

[161] S. A. Stern, Y. Mi, H. Yamamoto, and A. K. St. Clair, "Structure/permeability relationships of polyimide membranes. Applications to the separation of gas mixtures," *J. Polym. Sci. Part B Polym. Phys.*, vol. 27, no. 9, pp. 1887–1909, 1989.

[162] J. C. Grunlan, A. Grigorian, C. B. Hamilton, and A. R. Mehrabi, “Effect of clay concentration on the oxygen permeability and optical properties of a modified poly(vinyl alcohol),” *J. Appl. Polym. Sci.*, vol. 93, no. 3, pp. 1102–1109, Aug. 2004.

[163] D. Sikdar, D. R. Katti, K. S. Katti, and R. Bhowmik, “Insight into molecular interactions between constituents in polymer clay nanocomposites,” *Polymer (Guildf).*, vol. 47, no. 14, pp. 5196–5205, Jun. 2006.

[164] G. G. Kapantaidakis, S. P. Kaldis, X. S. Dabou, and G. P. Sakellaropoulos, “Gas permeation through PSF-PI miscible blend membranes,” *J. Memb. Sci.*, vol. 110, no. 2, pp. 239–247, 1996.

[165] M. Etxeberria, P. Corengia, S. Miguel, J. Zuniga, E. Fernandez-Gesalaga, and P. Jimenez, “Polysulfone and polyimide hollow fiber gas separation membrane preparation and module manufacturing,” *Procedia Eng.*, vol. 44, pp. 791–792, 2012.

[166] G. C. Kapantaidakis, S. P. Kaldis, G. P. Sakellaropoulos, E. Chira, B. Loppinet, and G. Floudas, “Interrelation Between Phase State and Gas Permeation in Polysulfone / Polyimide Blend Membranes,” vol. di, pp. 2788–2798, 1999.